

國立交通大學

光電系統研究所

碩士論文

側向電場用於電泳顯示器之應用與特性探討

Using Lateral Electric Field in Electrophoretic Displays for
Mechanism Understanding and Applications

研究生：許博鈞

指導教授：黃乙白 博士

鄭協昌 博士

中華民國一百零一年七月

側向電場用於電泳顯示器之應用與特性探討

Using Lateral Electric Field in Electrophoretic Displays for
Mechanism Understanding and Applications

研究生：許博鈞

Student : Po-Chun Hsu

指導教授：黃乙白

Advisor : Yi-Pai Huang

鄭協昌

Advisor : Shie-Chang Jeng



國立交通大學

光電系統研究所

碩士論文

A Thesis

Submitted to Institute of Photonic System

College of Photonics

National Chiao Tung University

in partial Fulfillment of the Requirements

for the Degree of

Master

in

Photonic System

July 2012

Hsinchu, Taiwan, Republic of China

中華民國一百零一年七月

側向電場用於電泳顯示器之應用與特性探討

碩士研究生： 許博鈞¹

指導教授： 黃乙白² 副教授 與 鄭協昌³ 助理教授

國立交通大學¹光電系統研究所²顯示科技研究所 以及³影像與生醫光電研究所

摘要

利用 In-Plane 電極製造橫向電場，與使用顯微鏡以微觀的觀測方式量測電泳式顯示器中微米粒子的運動情形，並運用 MATLAB 進行影像處理，以取出實驗所需的三種重要參數(飄移速度、粒子排列對比以及擴散速度)用以比較各種基礎波型的特性，進而得到粒子運動時的受力情形，並推導出運動時的受力模型，最後則可運用此特性改善電泳式顯示器之反應速度、雙穩態以及對比度。另外在橫向的觀測中，亦可與一般縱向的驅動作出關聯。

除此之外，亦可利用橫向電場進行電泳式顯示器的驅動，使用橫向電場進行重置，則可於近乎無閃爍的狀態之下將正負離子中和進而得到更佳的雙穩態，並運用橫向電場，先行布置粒子位置而得到更快的反應時間。此外，可以以單通道或雙通道的訊號進行更高精細度的灰階調控，用以實現高灰階數以及降低殘影的成果。

當然，由於在此種基板設計下，雙穩態與殘影的問題即可大大縮小。若可將流體更換為較低粘滯係數之材料，另可以得到更快的反應時間亦不會使得整個電泳式顯示器的顯示品質降低太多。所以，未來可以由材料、驅動波形以及電極的形狀進行搭配並優化，以得到高品質之電子紙。

Using Lateral Electric Field in Electrophoretic Displays for Mechanism Understanding and Applications

Student: Po-Chun Hsu¹ Advisor: Yi-Pai Huang² and Shie-Chang Jeng³

¹ Institute of Photonic System, College of Photonics

² Display Institute, College of Electrical and Computer Engineering

³ Institute of Imaging and Biomedical Photonics, College of Photonics

National Chiao Tung University

Abstract

We proposed a lateral observation method for mechanism understanding. The lateral observation method could observe the particle position and measure the parameters of driving characteristics such as drifting speed, particle packing, and bistability lost. In lateral direction, there was no information shielding by the other particles which were closer to the light source in vertical observation. The slow response time, non-perfect bistability, and improvable extreme state were issues in electrophoretic display system. We could find out how the internal electric force affected those issues and make a solution.

On the other hand, the lateral driving method provided us another way to switch images. Using lateral reset could be a non-flicker reset for comfortable reading and enhance the transition time by separation the particles. Furthermore, dual side driving could build up a total different electric field in the same electrode for applications. Single side driving could fine tune the lightness by the curved and weak electric field. Double side driving could coarse tune the lightness in a short time. The number of gray levels and short term bistability could be increased.

Acknowledgements

首先，要誠摯的感謝實驗室兩位老師，謝漢萍教授和指導老師黃乙白副教授在碩士兩年的求學生涯中提供豐富的實驗室資源和良好的研究環境。對於研究過程、研討會報告與英文能力的指導鞭策，培養我進入社會後所應具備的基本條件。也由衷感謝各位口試委員對於本論文所提供的寶貴建議，使整體內容更加趨於完備。

此外，更感謝林芳正助理研究員，在碩士生涯的指導與帶領，無論是對於論文研究方向上的建議、在研究過程中遇到問題時的指導與幫忙、研討會報告與論文的修改，還有精神上的鼓勵與打氣等，同時身為 FSC 與電子紙組別的支柱實在是非常辛苦。學長除了具備超群的文書處理能力、表達能力，對於研究的熱誠與專業是讓我最佩服之處，也成為我的學習榜樣。除此之外也謝謝同組已畢業的學姊吳思頤與同學楊上翰在研究上的合作與幫忙，與你們一起實驗與問題討論是很振奮人心的事情。也謝謝合作計畫公司的同仁楊柏儒、張明仁、黃若城學長，對於研究與實驗方向上面的建議、協助與配合，使得一切能夠順利流暢的進行。

感謝實驗室台翔、精益、國振、凌堯、柏全、奕智、小皮、大頭、致維哥、與志明等博班學長姐，提供各方面專業的指導與意見。也特別感謝上一屆學長姐小馬、小頭、立偉、馬志堯、董哥、蓋 B、昌毅、小 fighter、博六、子寬和江濟宇等人，在我碩一時的照顧。此外也謝謝碩二的同學張綺、拉拉、博凱、白諭、周秉彥、光電王子王柏皓、罔務以及師父，在這兩年中無論是在研究、課業和生活上一起打拼與互相扶持，讓實驗室增添許多趣味。另外，也要向實驗室的雅惠、穎佳、茉莉、江介堯和蓮芳五位助理們還有學弟妹們表達最誠摯的感謝，讓我們在研究之餘無後顧之憂，並使實驗室整體像一個大家庭一樣隨時充滿歡愉的氣氛。最後，對於我的家人及朋友們，感謝你們這兩年來背後的關懷、鼓勵與陪伴，使我能夠無後顧之憂且順利地完成兩年的碩士學位，這份感激與喜悅要分享給所有認識和幫助過我的人。

Table of Contents

摘要	iii
Abstract	iv
Acknowledgements	v
Chapter 1. Introduction	1
1.1 Classification of E-papers.....	2
1.1.1 The Transmissive Type E-paper.....	2
1.1.2 Organic Light Emitting Diode.....	3
1.1.3 Mirasol Display	4
1.1.4 LC E-paper	5
1.1.5 Electrophoretic Display	6
1.2 The Types of Electrophoretic Displays.....	8
1.2.1 Microcapsule Electrophoretic Display	8
1.2.2 Quick Response Liquid Powder Display.....	9
1.2.3 Microcup Electrophoretic Display.....	10
1.3 Motivation and Objectives.....	11
1.4 Prior Arts of Lateral Electrode Design	12
1.5 Thesis Organization	13
Chapter 2. Mechanism	15
2.1 The Phenomena of Electrophoresis	15
2.1.1 The Formation of Charged Particle	15
2.1.2 The Electric Double Layer and Zeta Potential	16
2.1.3 Electrostatic and DLVO Theorem	19
2.1.4 The Bistability State	21
2.2 The Non-perfect Image Effect.....	22

2.2.1	Paging Time	22
2.2.2	The Remnant DC	23
Chapter 3.	Equipment & Method	25
3.1	Equipments	25
3.1.1	Photo Diode	25
3.1.2	Photometer	26
3.1.3	Function Generator	27
3.1.4	Laser Scanning Confocal Microscope	28
3.2	Observation System	29
3.2.1	The Macroscopic System Setup	29
3.2.2	The Microscopic System Setup	29
3.3	Evaluation Indexes	31
3.3.1	Particle moving velocity $v(t)$	32
3.3.2	Particle Packing Contrast	32
3.3.3	Lateral Bistability (Repulsing speed)	33
Chapter 4.	Simulations	34
4.1	Simulation Tool	34
4.2	Simulation for Electric Field Distribution	35
4.3	Simulation for Hydromechanics	37
4.4	Optimization for Real Product Case	38
Chapter 5.	Experimental Results	42
5.1	Mechanism Confirmation	42
5.1.1	Experiment of Moving Velocity $v(t)$	43
5.1.2	Experiment of Packing Contrast	44
5.1.3	Experiment of Bistability (Repulsing Speed)	46
5.1.4	Microcup System Force Model	47

5.1.5	Correlation with Lateral and Vertical	49
5.2	Application Proposition.....	51
5.2.1	Lateral Reset.....	52
5.2.2	Dual Side Driving Characteristic.....	54
5.3	Summary.....	62
Chapter 6.	Conclusion and Future Work.....	64
6.1	Conclusion.....	64
6.2	Remnant Issue and Future Work.....	68

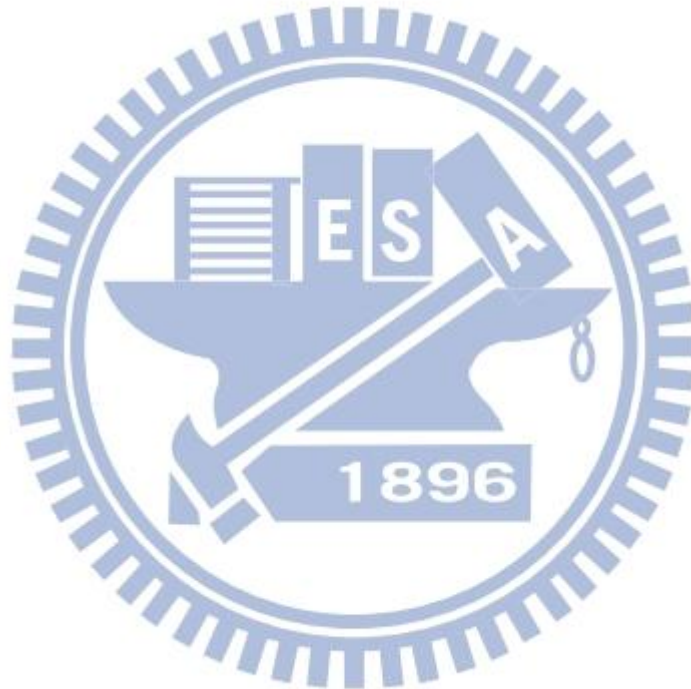


Figure Captions

Fig. 1-1 E-paper products (a) E-books. (b) Flexible displays. (c) Price tags. (d)Smart cards.	1
Fig. 1-2 The e-paper technologies including reflectivity and contrast ratio.....	2
Fig. 1-3 The prior arts of e-paper technologies.	3
Fig. 1-4 The structure of the OLED.	4
Fig. 1-5 Mirasol display working principle.	4
Fig. 1-6 The principle for BiNem with different driving pulse.	5
Fig. 1-7 The principle for ChLC shows the image.	6
Fig. 1-8 EPD can be read under sunlight and LCD will see nothing.	7
Fig. 1-9 When switching pages the previous image still remaining.....	7
Fig. 1-10 After several hours the bright region became darker and vice versa.	7
Fig. 1-11 The display method in microcapsule EPD.	9
Fig. 1-12 The QR-LPD structure.....	9
Fig. 1-13 The microcup EPD structure.....	10
Fig. 1-14 The operation principle of microcup EPD.....	11
Fig. 1-15 The comb-like electrode for the lateral electric field.....	12
Fig. 1-16 The main lateral electric field functions.	13
Fig. 2-1 The diagram for phenomena of electrophoresis.....	15
Fig. 2-2 The surfactant working function.....	16
Fig. 2-3 Scheme of the ion distribution around the charged particle. The gray circle is the charge density around TiO ₂ , the darker the denser.	18
Fig. 2-4 Potential variation with distance for a charged surface: (a) potential reversal due to adsorption of surface, (b) adsorption of surface.	19
Fig. 2-5 The Chart of DLVO theory.	20

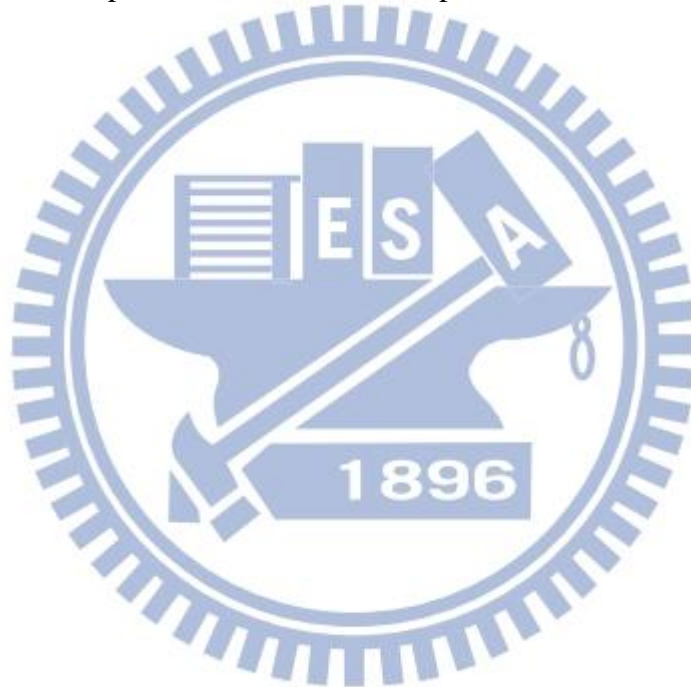
Fig. 2-6 Schematic showing paging time effect.	22
Fig. 2-7 Schematic showing remnant DC effect.....	23
Fig. 3-1 The photoelectric effect.	26
Fig. 3-2 The PDA100A photo diode.....	26
Fig. 3-3 The Photometer, I-one.....	27
Fig. 3-4 The Agilent 33210A function generator.....	27
Fig. 3-5 The IX71 laser scanning confocal microscope.	28
Fig. 3-6 The light path in macroscopic system.....	29
Fig. 3-7 The light path of the microscope system.	30
Fig. 3-8 The flow chart of MATLAB programming.	31
Fig. 3-9 (a) The top view of the video was picked up frame by frame in transmissive mode. (b) The white track was the particle motion in different time along X direction.	32
Fig. 3-10 The top view of the cell. Black and white area has high concentration of black and white particles respectively. Yellow area has few particles.	33
Fig. 4-1. The cross section of electric distribution in the cell, working ratio is defined as A_{working} (red dashed square)/ A (yellow solid square).	35
Fig. 4-2 (a) The conditions with L fixed at 100 μm . (b) W fixed at 50 μm . Red curves are electric field along the lateral direction. Blue ones are working ratio.....	36
Fig. 4-3 The electric field distribution in W= 50 μm L= 200 μm lateral operation.	36
Fig. 4-4 The particle flow in W = 50 μm L = 200 μm lateral operation.	37
Fig. 4-5 The velocity strength in W = 50 μm L = 200 μm lateral operation.	38
Fig. 4-6 Normalized working ratio with acceptable electric field ($E_x > 0.3 \text{ V}/\mu\text{m}$)	39
Fig. 4-7 The voltage distribution in W = 5 μm L = 20 μm lateral operation.	39
Fig. 4-8 The electric field distribution in W = 5 μm L = 20 μm lateral operation....	40

Fig. 4-9 The velocity distribution in $W = 5 \mu\text{m}$ $L = 20 \mu\text{m}$ lateral operation.	41
Fig. 4-10 The velocity field distribution in $W = 5 \mu\text{m}$ $L = 20 \mu\text{m}$ lateral operation.	41
Fig. 5-1 The basic waveforms are DC, shaking, and pulsing.	42
Fig. 5-2 The curves including different driving time and waveforms are plotted as the particles maximum speed.	43
Fig. 5-3 The particle packing contrast versus voltage curves are plotted containing different driving time and waveforms.	45
Fig. 5-4 (a) Short term bistability (b) long term bistability including different driving time and waveforms are plotted in versus voltage.	46
Fig. 5-5 The forces happened when diving.	48
Fig. 5-6 The screening field caused the repulsive electric field.	48
Fig. 5-7 The stable state force evolution.	49
Fig. 5-8 The optical responses in different voltage at vertical direction.	50
Fig. 5-9 The expected model forms the gray levels with white and black particle. (a) The optical response was not dominated by the concentration of the particles. (b) Different voltage packed the different purity of particles.	50
Fig. 5-10 The lateral driving method setup.	51
Fig. 5-11 The lateral reset waveform by the opposite polarity in signal 1 and 2.	52
Fig. 5-12 The lateral reset could prevent collision by separating the particles.	52
Fig. 5-13 The comparison of reset waveform.	53
Fig. 5-14 The particles moving in the lateral reset.	53
Fig. 5-15 Comparison of improved driving and vertical driving (a) Improved image transition including reset waveform (b) Vertical driving including reset.	54
Fig. 5-16 The particles transition in reset waveform.	54
Fig. 5-17 The single side driving (a) waveform and (b) perturbs the lightness.	55

Fig. 5-18 The electric field distribution in single side driving.	56
Fig. 5-19 The double side driving (a) waveform and (b) optical response.	56
Fig. 5-20 The electric field distribution in double side driving.	57
Fig. 5-21 The 30 volt double side driving (a) waveform and (b) optical response ..	58
Fig. 5-22 The double side driving (a) waveform with 15 and 30 volt pulsing after 30 volt DC and (b) optical response.	59
Fig. 5-23 The mixture waveform.	60
Fig. 5-24 Comparison of vertical driving and improved driving (a) Flicker and response time (b) Bistability.	61
Fig. 6-1 The proposed waveform for quick response, high contrast ratio and stable lightness.	65
Fig. 6-2 The particles transition direction.	66
Fig. 6-3 The coarse adjustment.	66
Fig. 6-4 The fine adjustment.	67
Fig. 6-5 The gray level transition web.	68

List of Tables

Table 1-1 The prior arts of EPD.	8
Table 2-1 Magnitudes of the characteristic force when temperature is 300K, particle diameter is 1 μ m, surface electric potential is 5V, velocity is 1 μ m/s, density is 10 ³ kg/m ³ and viscosity is 10 ⁻³ Pa· s.....	21
Table 5-1 The comparison of conventional and In-Plane EPDs.....	62
Table 6-1 The effects of W and L in the microcup EPD.....	64
Table 6-2 The improvement of the microcup EPD.....	67



Chapter 1. Introduction

Nowadays, green technology becomes more and more popular. Especially, green display technology is one of the most popular technologies in the world. The electrophoretic display (EPD) [1] has been regarded as one of the dominant technologies of E-paper in the green display technology. It has several advantages such as wide viewing angle, operation without backlight, readability in sunlight ambience, flexibility and unbreakability. It can be not only low power consuming but also thinner and lighter.

Some companies have invested in the e-paper technology for years, such as AUO, Bridgestone, Qualcomm, Fujitsu, and Philips. They have put a lot of people and money to win the competition of e-paper. Therefore, many e-paper technologies were developed quickly and the products were manufactured for living needs as shown in Fig. 1-1



Fig. 1-1 E-paper products (a) E-books. (b) Flexible displays. (c) Price tags. (d) Smart cards.

1.1 Classification of E-papers

There are lots of E-paper technologies in the world as shown in Fig. 1-2. Generally, the technologies are divided into two kinds: lighting (transmissive or emissive) and reflective type. The lighting ones have the better image quality, and the other ones provide the comfortable reading experiment.

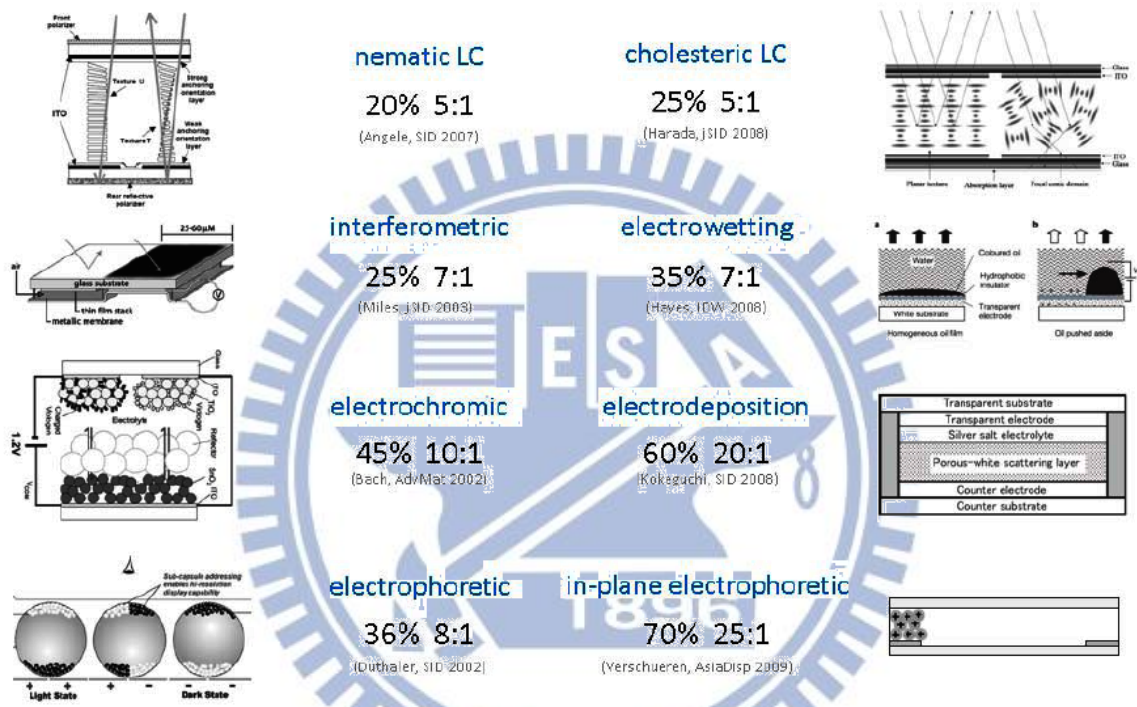


Fig. 1-2 The e-paper technologies including reflectivity and contrast ratio.

1.1.1 The Transmissive Type E-paper

The transmissive and emissive types function as liquid crystal displays (LCDs) or organic light emitting diodes (OLEDs) having 8-bit gray levels, higher contrast ratio, wide color rendering and fast response time which make them possible to play videos. However, the viewing angle of LCD is limited and this technology has color shift issue. Nevertheless, its power consumption is higher and it cannot be seen clearly under sunlight ambience because the luminance of the backlight is weaker than sunlight. The reflective type usually

makes people comfortable just like reading a paper, and has the benefit in power consumption. These superiorities make people able to read for a long time and it can replace the book in next generation. Therefore, the most popular technologies of the E-paper are Mirasol display, LC E-paper, and EPD as shown in Fig. 1-3.

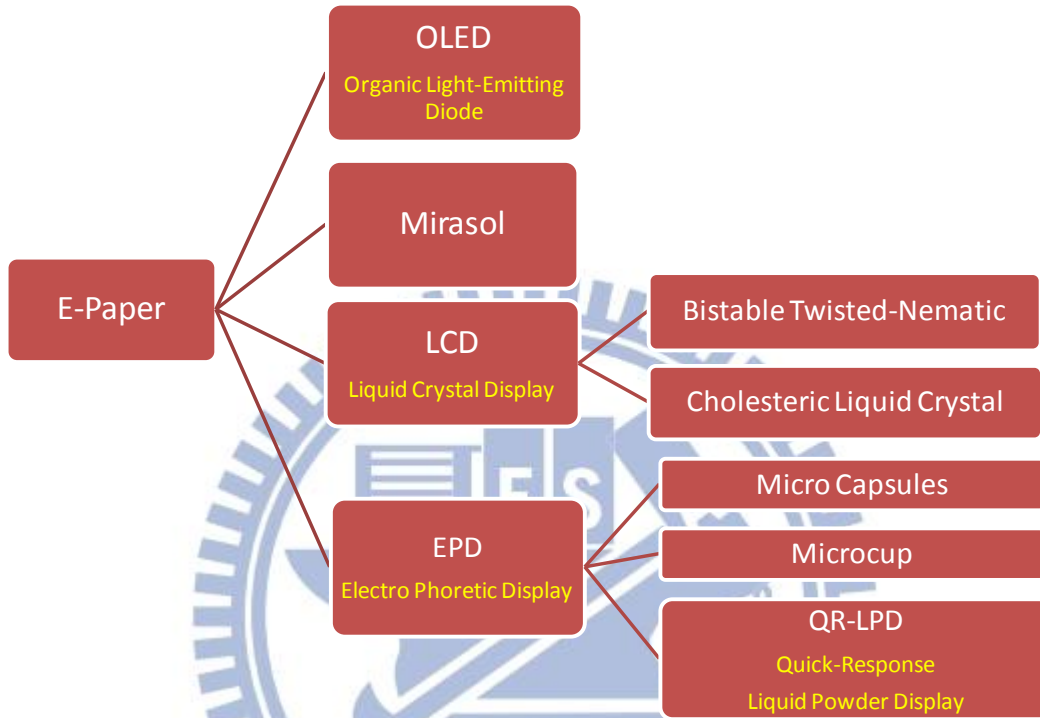
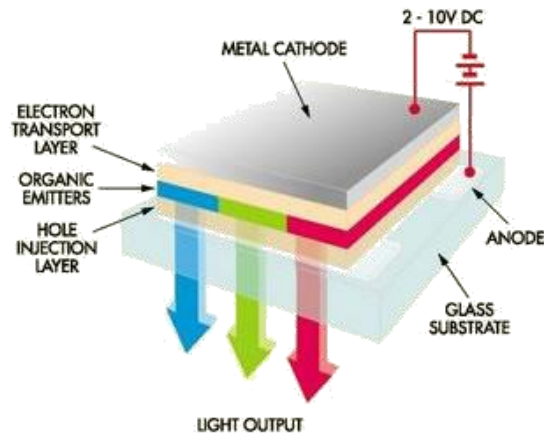


Fig. 1-3 The prior arts of e-paper technologies.

1.1.2 Organic Light Emitting Diode

Organic light emitting diode (OLED) [2] is a device without viewing angle limitation and has high brightness because of self-emissive as shown in Fig. 1-4. It can be operated without backlight and ambient light. It lights when electron and hole are combined, so the response time is fast. However, OLED still has some disadvantages, such as short life time, high cost, difficulty to manufacture and unfavorable sunlight readability.



http://quanta.hanyang.ac.kr/Education/Education_OLED_Principles.htm

Fig. 1-4 The structure of the OLED.

1.1.3 Mirasol Display

Mirasol display [3] was invented by Mark W. Miles, a MEMS researcher and founder of Etalon, Inc., and co-founder of Iridigm Display Corporation. The principle of Mirasol is using interference of light by micro electro mechanical system (MEMS) as shown in Fig. 1-5. It has fast response time, colorful image and low power consumption with bistability. By using the MEMS fabrication process, Mirasol display is very expensive.

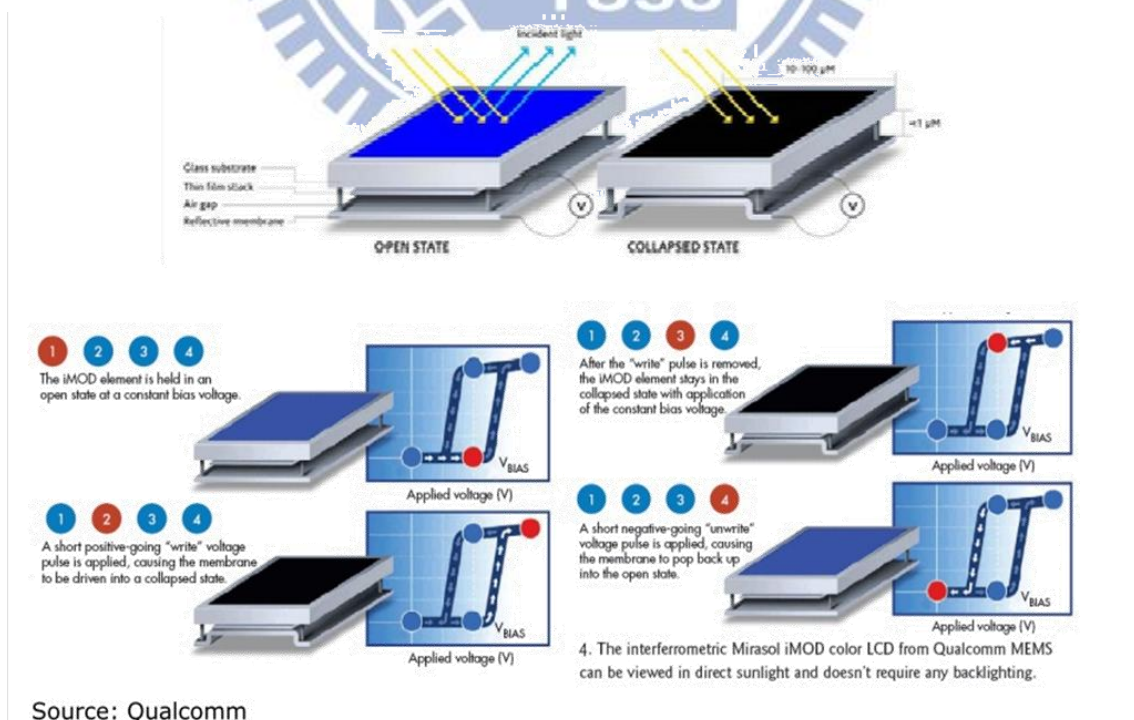
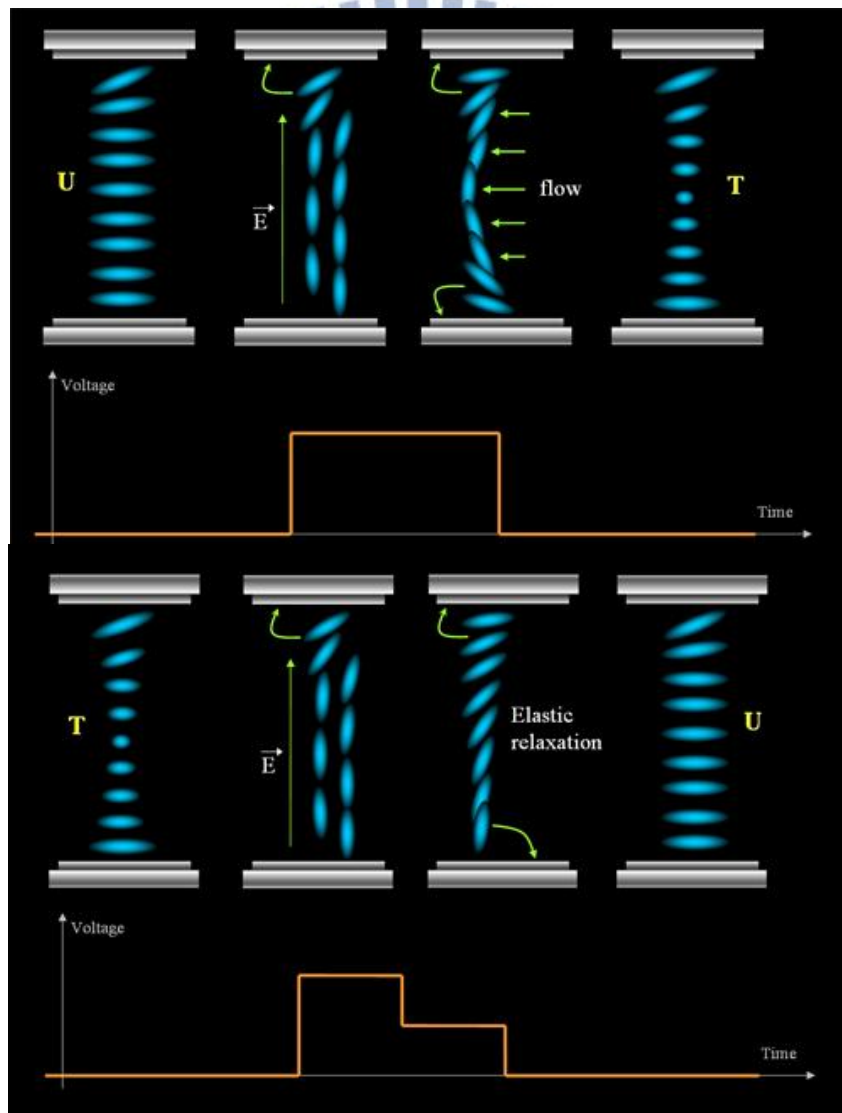


Fig. 1-5 Mirasol display working principle.

1.1.4 LC E-paper

LC e-paper can be classified into two types: bistable LC and cholesterol LC (ChLC). In bistable LC type, BiNem [4] is a breakthrough technology that enhances existing LCD technologies by providing a memory effect and superior image quality. It is based on a unique principle called “surface anchoring breaking” fully patented by Nemoptic. BiNem technology has two stable states, the Uniform (U) state and the Twisted (T) state as shown in Fig. 1-6.



<http://www.personal.kent.edu/~mgu/LCD/binem.htm>

Fig. 1-6 The principle for BiNem with different driving pulse.

The other one is ChLC [5] which is a type of liquid crystal with a helical structure and it is therefore chiral. The operation principle is that lights are reflected in the planar texture to reveal the bright state, while lights transmit and are scattered in the focal conic texture and reveals dark state as shown in Fig. 1-7.

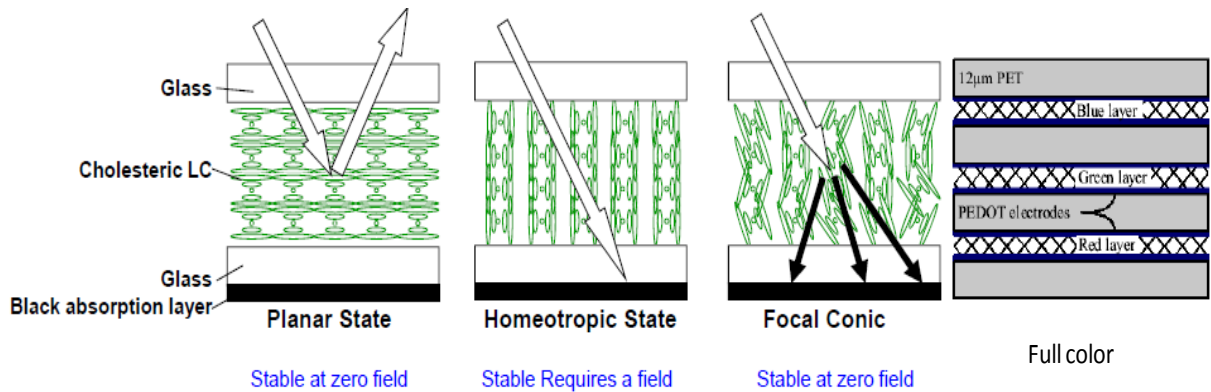


Fig. 1-7 The principle for ChLC shows the image.

1.1.5 Electrophoretic Display

EPDs usually show the image by manipulating the position of black and white charged particles [14]. The charged particles are prepared with the pigments mixing with the surfactants in the non-polar solvent [15]. Upon applying an external electric field, the charged particles move along the electric field and display images by mixing the different percentage of particles [16].

EPD is a thin, light, robust, and flexible display, and is readability under the sunlight ambience as shown in Fig. 1-8. According to its bistability [6] characteristic, EPD requires a voltage only when switching the images. With this phenomenon, EPD is totally different from an e-paper using conventional LCDs and OLEDs. However, EPD still has some issues such as slow response time, flicking effect when changing the pages, ghost images as shown in Fig. 1-9 and non-perfect bistability as shown in Fig. 1-10.



Fig. 1-8 EPD can be read under sunlight and LCD will see nothing.

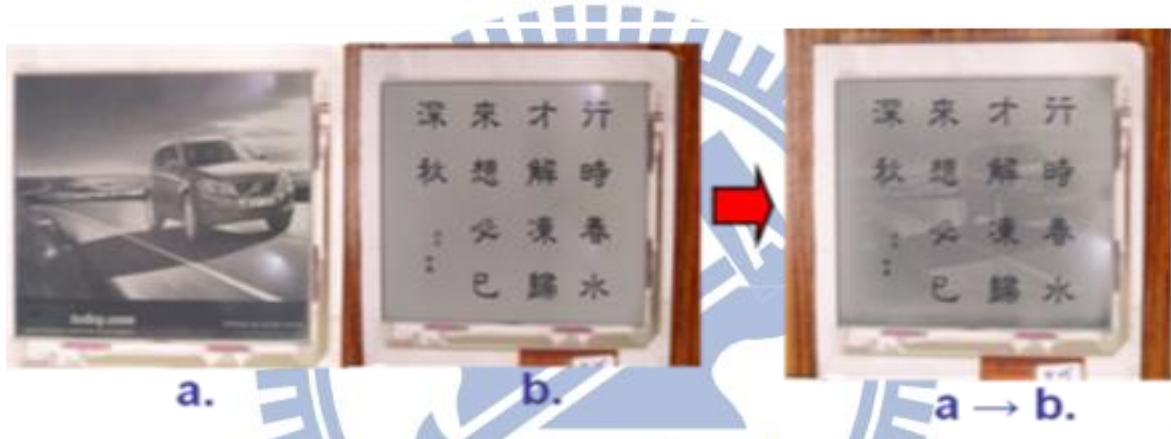


Fig. 1-9 When switching pages the previous image still remaining.



Fig. 1-10 After several hours the bright region became darker and vice versa.

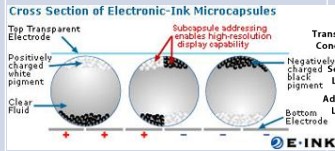
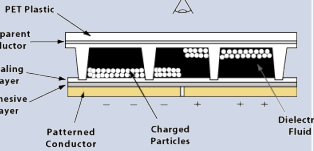
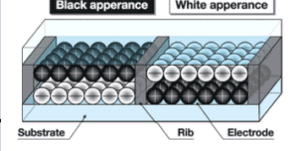
In those technologies, EPD is the best for human, because it has the same characteristics as paper. The contrast ratio of EPD is about 10 and it is the reflective type

display. Moreover, EPDs' reflectivity is the highest one in the E-paper products. On the other hand, as a reader, EPD has zero power consumption when the image was not changing because of the bistability. It only consumes the electricity when image switches.

1.2 The Types of Electrophoretic Displays

The electrophoretic display (EPD) is regarded as one of the dominant technologies of E-papers in green display technologies. There are three main EPD skills in Table 1-1.

Table 1-1 The prior arts of EPD.

	Microcapsule EPD	Microcup EPD	QR-LPD
Driving Method			
Reflectivity	50%	40%	40%
Transition Time	~300ms	~300ms	0.2ms
Driving Voltage	±15V	±15V	~70V
Driving	AM/PM	AM/PM	PM
Contrast Ratio	10:1	10:1	10:1
Color	by color filter	by color solvent	by color filter
Company	E-INK	SIPIX	Bridgestone

1.2.1 Microcapsule Electrophoretic Display

The microcapsule EPD [7]-[9] is invented in MIT and produced by E-ink Company. It has microcapsules which load the black and white opposite charged particles to form the different reflectivity as shown in Fig. 1-11. When the bottom electrode was exerting positive voltage, the negative particles would swim to the bottom, vice versa.

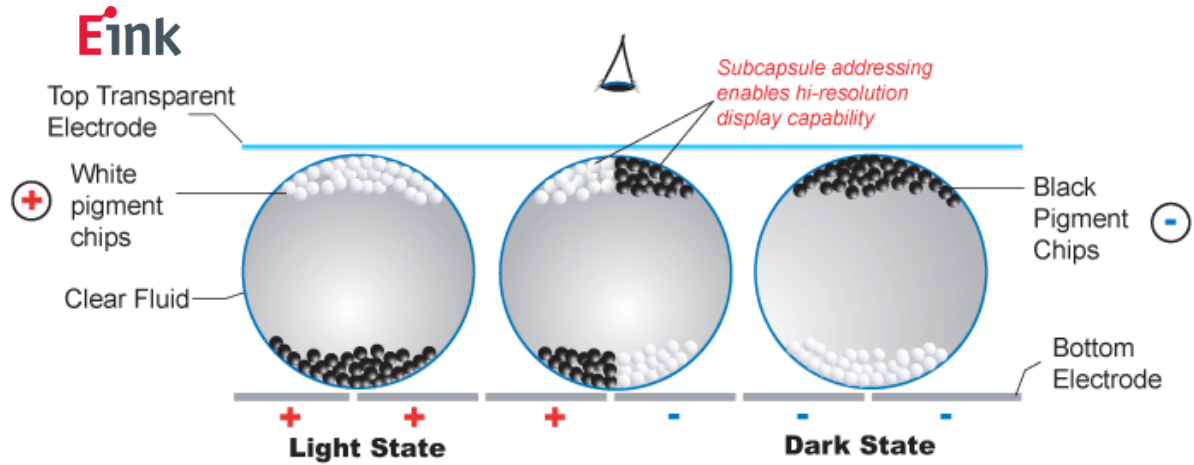
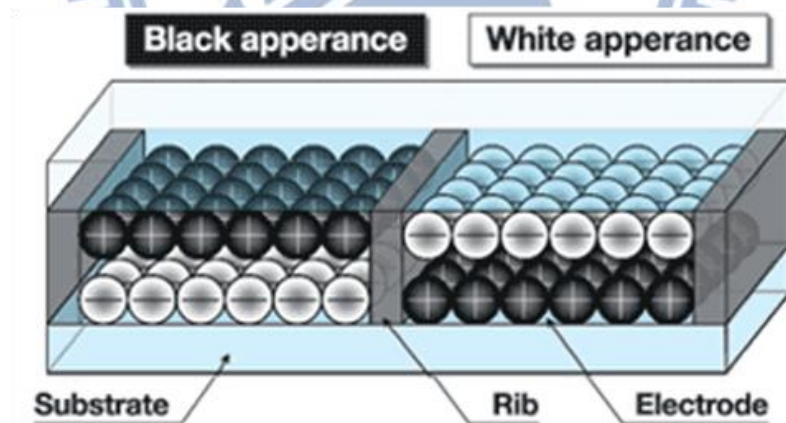


Fig. 1-11 The display method in microcapsule EPD.

1.2.2 Quick Response Liquid Powder Display

The quick response liquid powder [10][11] (QR-LPD) display is proposed by Bridgestone Company. This kind of technology uses the opposite charged white and black particles in the dry type as powders as Fig. 1-12.



Source: Bridgestone

Fig. 1-12 The QR-LPD structure.

When applying voltage, the corresponding particles would flow downstream or upstream just like the microcapsule EPD. But the driving condition is totally different from the microcapsule EPD by the solid state powder and using air as a solution. By doing so, the

transition time is much faster than the other EPDs, but the driving voltage is too high to build on the active matrix.

1.2.3 Microcup Electrophoretic Display

The microcup EPD [12] is provided by SiPix Company. It is made up of matrix of cups typically 150 μm in width. The whole display has strong strengths because of the microcup structure which is more applicable in flexible displays and which fits into roll to roll manufacture. It can be made square or hexagon as shown in Fig. 1-13.

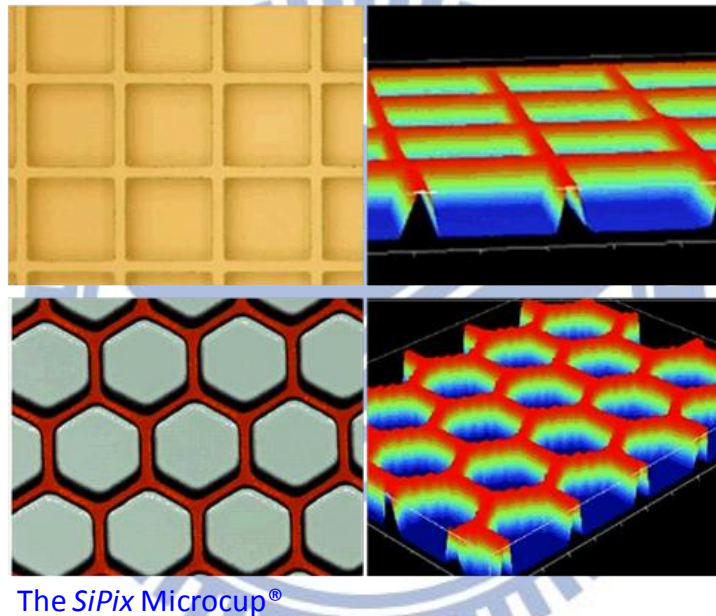


Fig. 1-13 The microcup EPD structure.

When bottom electrode was exerting negative voltage, the positive charged particles would swim to the bottom and the other side shows the fluid in black. In other words, when bottom electrode was exerting positive voltage, the charged particle would swim along the electric field to the top of the microcup, and shows white as shown in Fig. 1-14.

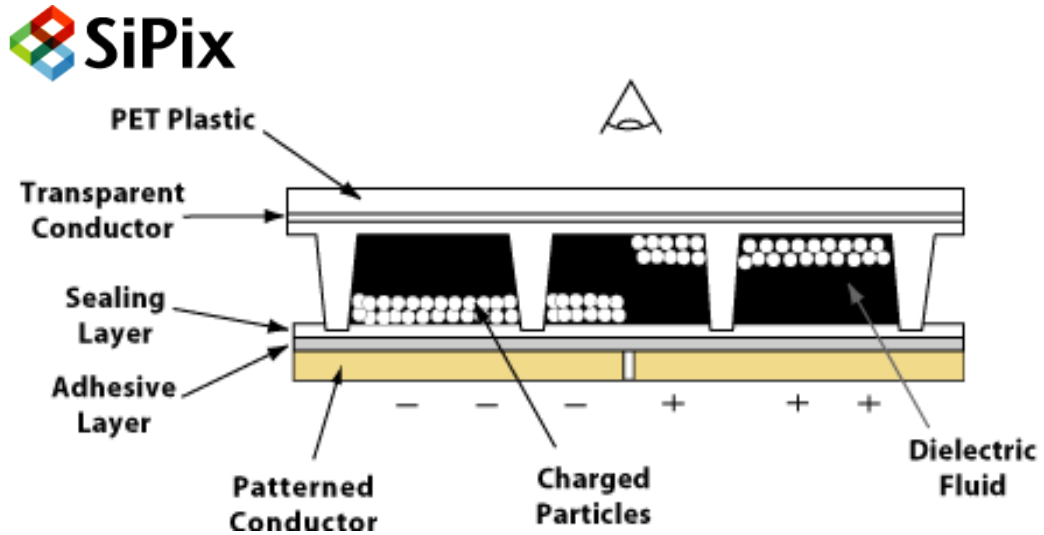


Fig. 1-14 The operation principle of microcup EPD.

Although the transition time of a microcup EPD is not fast enough compared to the QRLPD, the microcup EPD has lower manufacturing cost due to roll-to-roll process [13] and color can be realized by color solvent instead of inefficient color filters, which increases the overall whiteness. Therefore, the microcup EPD was chosen to be our research objective.

1.3 Motivation and Objectives

Since 1979, M. A. Hopper and V. Novotny proposed the EPD model by optical simulation and experiment, the model was modified several times in a half hundred years. In those models, the optical response was observed in such different ways to confirm the correctness of their model [16]-[19]. However, the electrophoresis happens in a micro meter scale, the macroscopic observation has less persuasiveness. Therefore, we want to use the microscopic observations to fully understand the mechanism in the electrophoretic display and develop the new application with lateral electric field in the microcup EPD by the comb-like electrode as shown in Fig. 1-15.

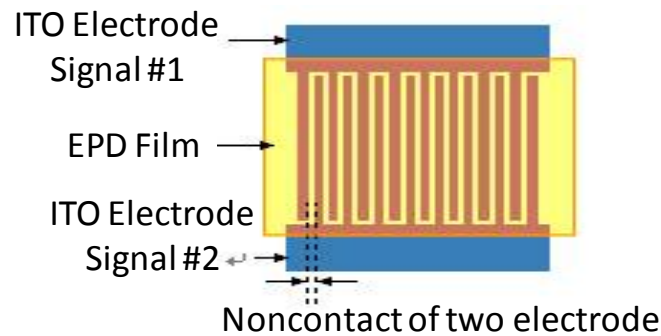


Fig. 1-15 The comb-like electrode for the lateral electric field.

On the other hands, EPD technology face difficult issues such as slow response time, ghost image, non-perfect bistability, paging time issue, and the flicking effect when switching the pages. We want to use both lateral and vertical electric field for more degree of freedom driving method to solve those issues. Flicker should be eliminated ($\Delta L^* < 1$) for comfortable reading, response time should be shorter than 500 ms for human patience in nowadays and short term bistability lost should be lower than $\Delta L^* < 1$ due to the human awareness. Because the trend of the green display is irresistible, this job is important and needed. We have had to solve those issues and formed the hopeful future.

1.4 Prior Arts of Lateral Electrode Design

The lateral electrode design is developed to switch the reflectivity by the shielding percentage in Philips Company and Canon Company or the mixture percentage in SiPix Company as shown in Fig. 1-16.

Canon used the mirror-like reflective substrate to form the white state, and put the black particle to shield the substrate to form the dark state [20]-[22]. The lateral electric field was used for driving the particles in or out the reflective region and to show the image.

Philips made the shielding region to hide the reflective particles to form the dark state. And they also made the transmissive region to show the particles to form the white state. When the lateral electric field was driven, the particles went in or out the shielding region to

switch the images, so that Philips used the lateral electrodes [23][24].

Also, SiPix Company proposed the electrophoretic display with dual mode switching [25][26]. Dual mode switching comprised the vertical and lateral directional electric field to form the more freedom driving method. This method not only prevented the undesired movement of the charged particles in the cell but also provided the high image quality. Moreover, with dual mode switching, the color EPD would be developed without color filter.

Philips and Canon used lateral electric field to form the image just because their image formation method was dominant by the area in X-Y plane. SiPix used lateral electric field to form the color image. They did not eliminate the flicking effect or internal electric field for the bistability and transition time.

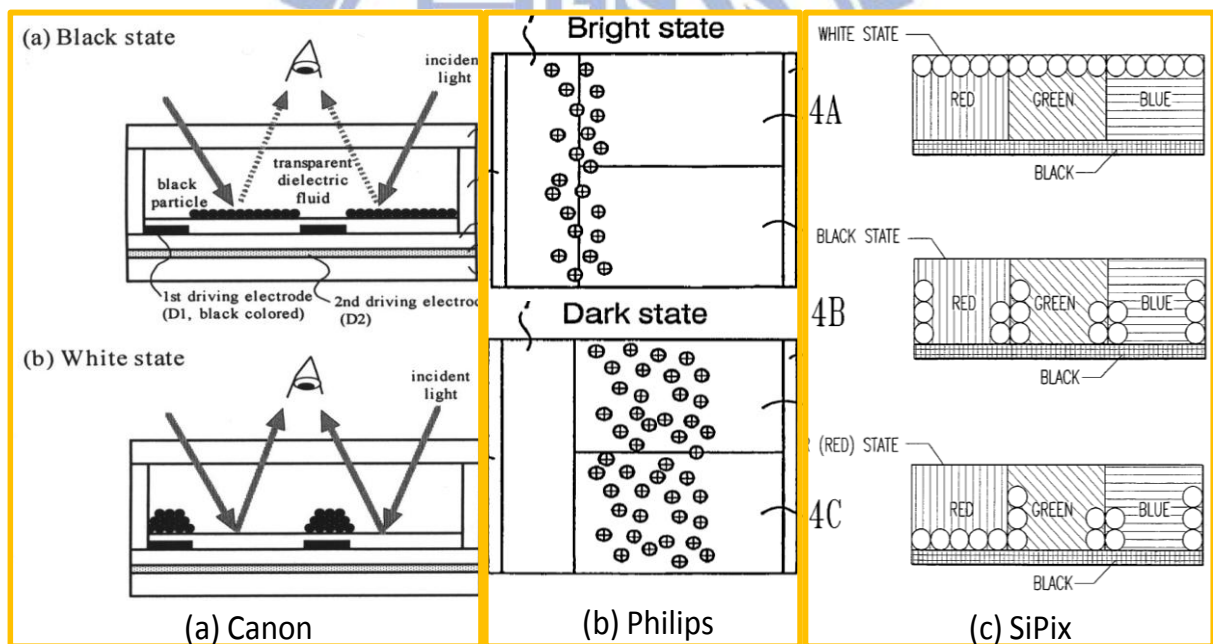


Fig. 1-16 The main lateral electric field functions.

1.5 Thesis Organization

The thesis is organized as follows: the fundamental properties, the charge and bistability mechanisms of a microcup EPD are introduced in Chapter 2. Besides, the

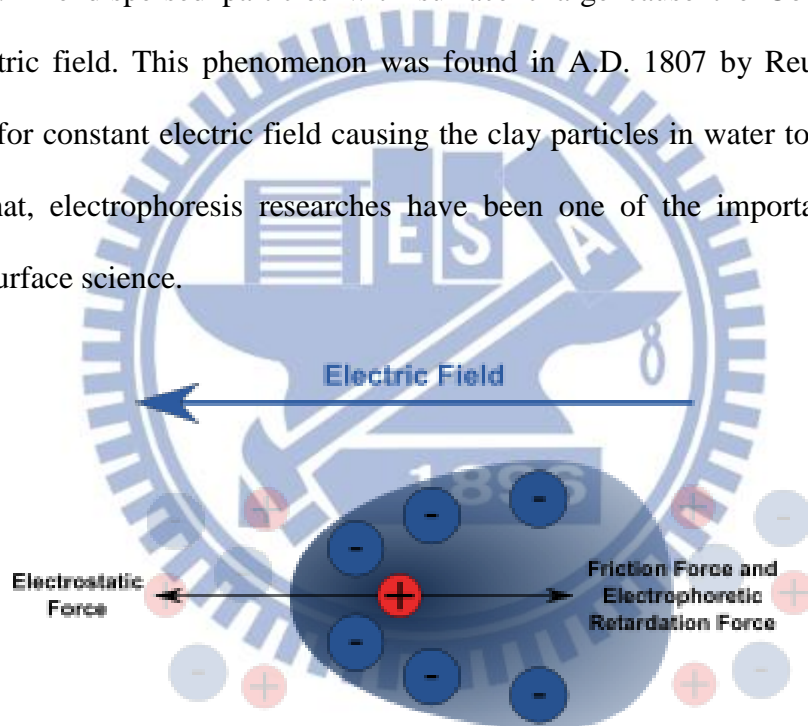
instruments used in the experiment and the measurement skills are described in Chapter 3. The simulation results of the electric field distribution for the electrode design are in Chapter 4, and experimental results and new driving method are discussed in Chapter 5. Finally, conclusion, minor issues and the future work are presented in Chapter 6.



Chapter 2. Mechanism

2.1 The Phenomena of Electrophoresis

There are four main types of electrokinetic in the fluid: electroosmosis, streaming potential, electrophoresis, and sedimentation potential [6]. Electrophoresis describes the motion of dispersed particles relative to the fluid under the influence of spatially uniform electric field. The dispersed particles with surface charge cause the Coulomb force by external electric field. This phenomenon was found in A.D. 1807 by Reuss, who do the experiments for constant electric field causing the clay particles in water to migrate as Fig. 2-1. After that, electrophoresis researches have been one of the important parts of the colloid and surface science.



<http://en.wikipedia.org/wiki/Electrophoresis>

Fig. 2-1 The diagram for phenomena of electrophoresis.

2.1.1 The Formation of Charged Particle

Making the charged particles was the first thing to make the electrophoretic environment. As the total charge was zero, the surfactant which has hydrophilic and hydrophobic ends was needed for charging the particles and solvent. Surfactant dissociates

and adsorbs on the different pigment to form the charged particles [27]. And some dissociated surfactant aggregates together forming the micelles [28] or anti-micelles as shown in Fig. 2-2.

The electric field could affect the particles with charge. On the other hands, the micelles and anti-micelles would be affected by the electric field too. Only the colored particle formed the image, yet the quantities of micelles and anti-micelles would influence the image quality because the micelles, anti-micelles and dissociated surfactant moves first, which make the internal electric field to stop the charged particles.

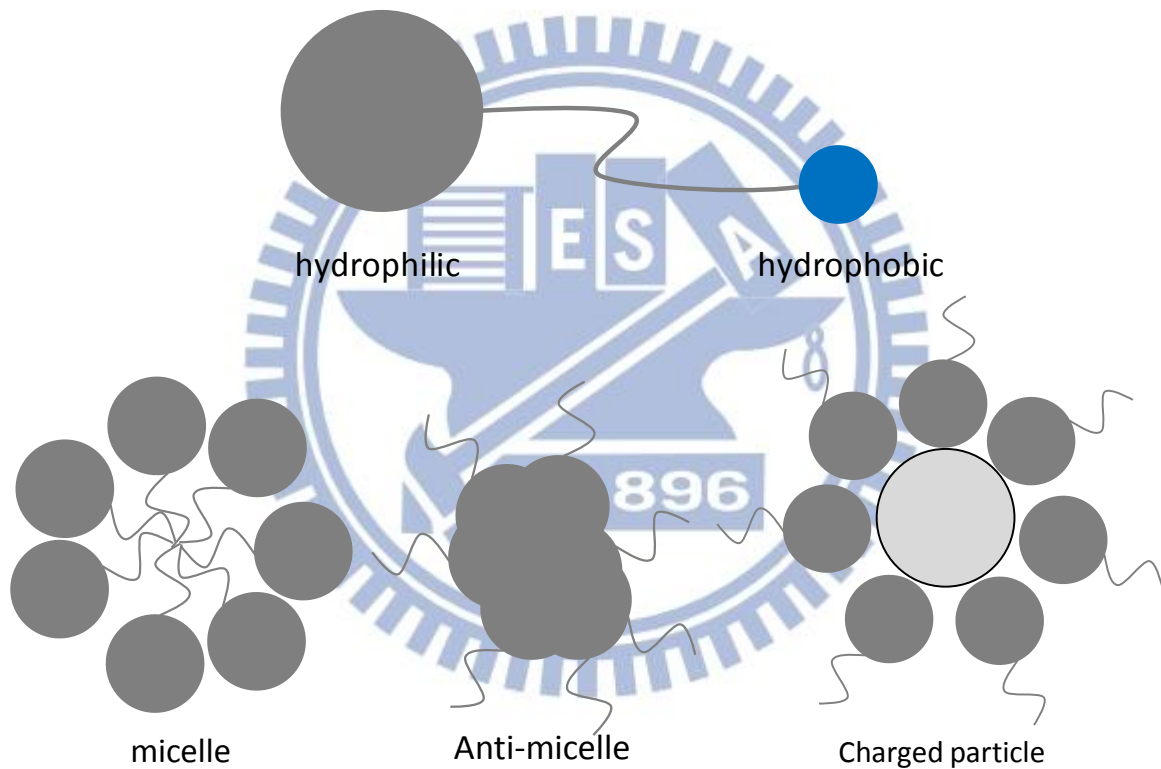


Fig. 2-2 The surfactant working function.

2.1.2 The Electric Double Layer and Zeta Potential

Colloid science [6] usually uses the electric double layer and zeta potential for describing the attractive or repulsive force. According to the Boltzmann distribution, the ion's position probability is proportional to the exponential to the power of energy as shown in Eq.(1) where z is valency, e is electron charge, ψ is potential, k is Boltzmann constant,

and T is temperature. For example, the black positive charged particle carried negative charged ion with high concentration outside formed a negative potential layer, called Stern layer. Then, the negative charged ions attached to the colloid continuously but blended some positive ions. This second layer is loosely associated with the object, because it is made of free ions which move in the fluid under the influence of electric attraction and thermal motion rather than being firmly anchored. It is thus called the diffuse layer.

$$P \propto e^{-\frac{ze\psi}{k_B T}} \quad (1)$$

When the spherical surface is considered, Poisson-Boltzmann equation is used to solve the problem. The formula was written as shown in Eq.(2), where r is distant, ψ is potential, z is valency, e is electron charge, n is ionic concentration, ϵ is permittivity, k is Boltzmann constant, and T is temperature. In this formula, there is no analytical solution, so Debye-Huckel approximation is needed.

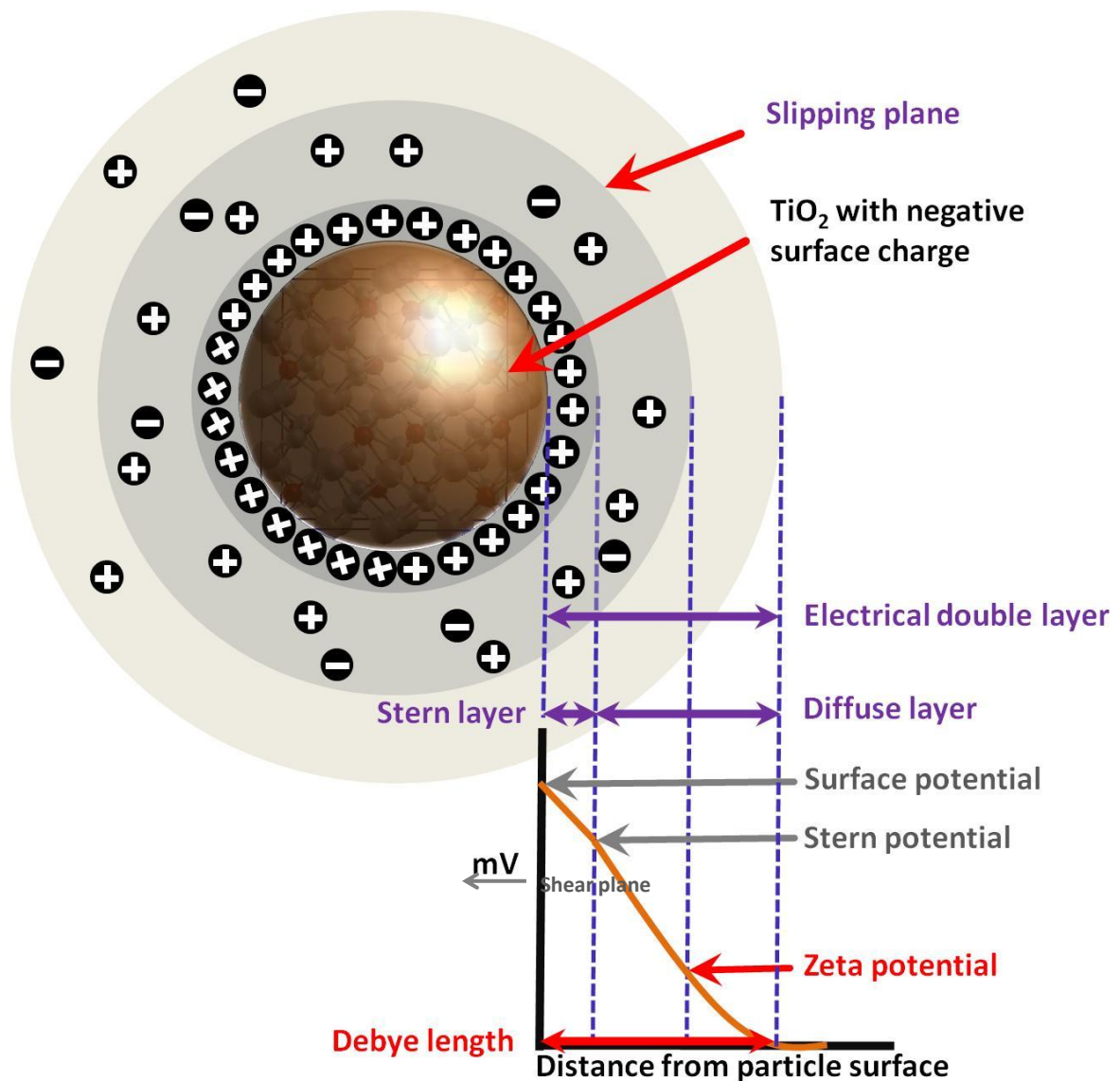
With Debye-Huckel approximation, $\kappa \equiv \left(\frac{2e^2 z^2 n}{\epsilon k_B T}\right)^{\frac{1}{2}}$ and $\Psi \equiv \frac{ze\psi}{k_B T}$ were defined.

Also, $r = a\left(1 + \frac{X}{\kappa a}\right)$ was substituted for thin double layer where $\kappa a \gg 1$ was assumed, and κ^{-1} meant the covered ions distance called Debye length. The formula can be rewritten as shown in Eq.(3), and the solution of energy distribution can be solved as shown in Eq.(4).

$$\frac{1}{r^2} \frac{d}{dr} \left(r^2 \frac{d\psi}{dr} \right) = \frac{2ezn}{\epsilon} \sinh\left(\frac{ze\psi}{k_B T}\right) \quad (2)$$

$$\frac{d^2\Psi}{dX^2} + \frac{2}{\kappa a\left(1 + \frac{X}{\kappa a}\right)} \frac{d\Psi}{dX} = \sinh\Psi \quad (3)$$

$$\Psi = \Psi_0 \frac{a}{r} e^{-\kappa(r-a)} \quad (4)$$

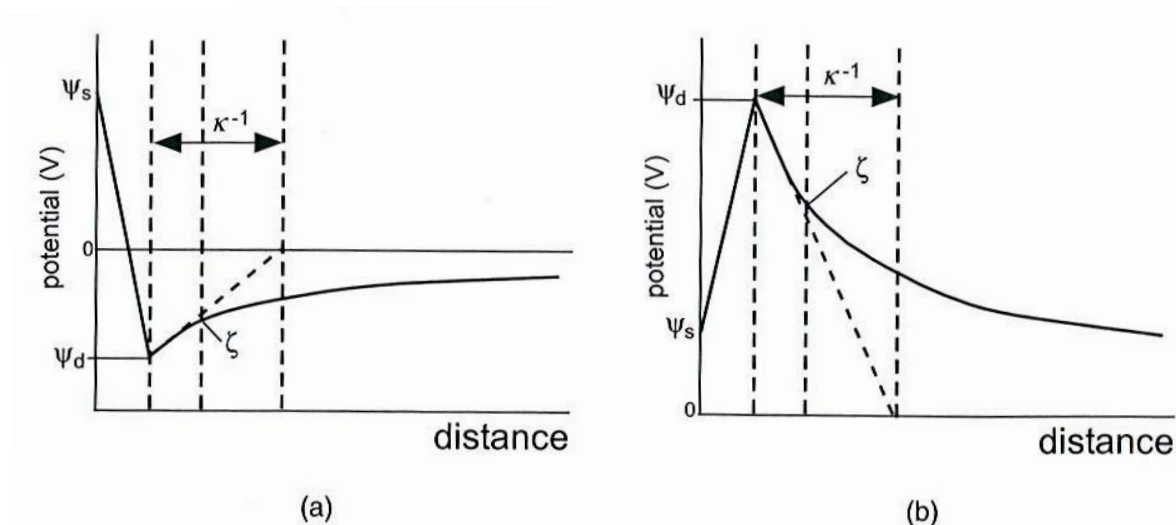


Source: S. I. Wu, "Electrokinetics of Charged-Particles in Microcup Electrophoretic Displays," NCTU, Master thesis (2011).

Fig. 2-3 Scheme of the ion distribution around the charged particle. The gray circle is the charge density around TiO₂, the darker the denser.

In real case, ions are of finite size and they can approach a surface to a distance not less than their radius. Ions form the diffuse mobile part of the electric double layer whose centers are located beyond the Stern plane. There is a surface which is located between one to two radii away from Stern plane referred to as the shear plane as shown in Fig. 2-3. The shear plane referred to the electrokinetic potential, called zeta potential. The zeta potential is marginally different in magnitude from the Stern potential, and electrophoretic potential measurements give the zeta potential of a surface.

It should be noted that adsorbed ions can have marked effects on the zeta potential when compared with the surface potential. The counterions can cause reversal of charge within the Stern layer as shown in Fig. 2-4, where ζ is zeta potential and κ^{-1} is Debye length. Therefore, the zeta potential does not give direct information about the surface potential when adsorbed ions are presented. As the zeta potential, the interaction due to the mobility would happen no matter when external or internal electric field was induced.



Source: Electrokinetic and Colloid Transport Phenomena, Jacob H. Masliyiah

Fig. 2-4 Potential variation with distance for a charged surface: (a) potential reversal due to adsorption of surface, (b) adsorption of surface.

2.1.3 Electrostatic and DLVO Theorem

In colloidal system, the interaction of particles is caused by attractive and repulsive forces. For systems, the electrostatic and van der Waal force are dominant in the stable environment. Therefore, if the system is in a stable state, the force should be balanced with electrostatic repulsion due to the electric double layer and dispersion attractive force by London-van der Waals force. The concept was proposed by Derjaguin, Landau, Verwey, and Overbeek at A.D. 1941 to A.D. 1948. It is called DLVO theory as shown in Fig. 2-5.

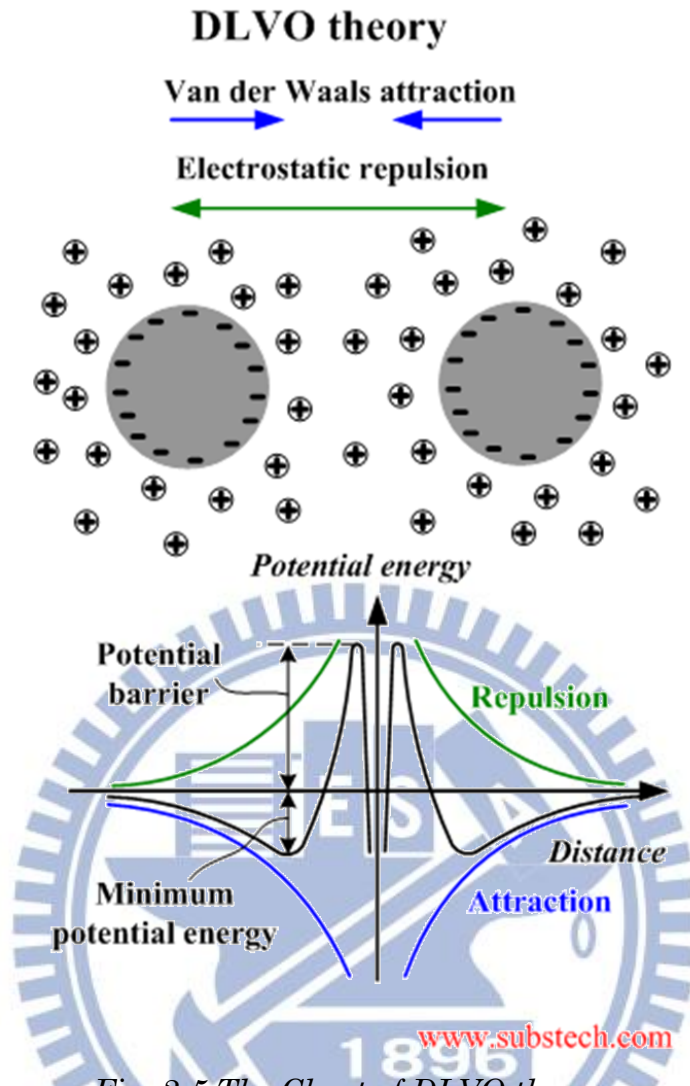


Fig. 2-5 The Chart of DLVO theory.

As electromagnetic theorem, applying the external electric field would cause the electric force described as $F = QE_{ex}$. And according to the Gaussian's law, the charge was calculated as shown in Eq.(5), where ζ is zeta potential and E_{ex} is external electric field. Therefore, the force with external electric field was solved as shown in Eq.(6).

$$Q = 4\pi\epsilon \int_a^{\infty} r^2 \left[\frac{1}{r^2} \frac{d}{dr} \left(r^2 \frac{d\psi}{dr} \right) \right] dr = 4\pi a \epsilon \zeta \frac{(1 + \kappa a)}{a} \quad (5)$$

$$F = 4\pi a \epsilon \zeta E_{ex} (1 + \kappa a) \quad (6)$$

2.1.4 The Bistability State

The bistability state was a more important factor for the EPD than the LCD. With bistability, image would not change without signals. It gives the comfortable reading experience and low power consumption.

Here is the way to keep the image stable: stop the particles by force balance as Section 2.1. With the balance force, the pigments would not move heavily, so that the image could be the same. There are several forces in the electrophoretic system: external electric force, internal electric force, viscosity, surface tension, gravitational force, buoyancy, van der Waal force between each particle, and Brownian's motion. The magnitude order of each force is shown in Table 2-1, the electrical force is the most important of all when driving and holding the image [29]. Therefore, how to adjust electric field is an essential art.

Table 2-1 Magnitudes of the characteristic force when temperature is 300K, particle diameter is 1 μ m, surface electric potential is 5V, velocity is 1 μ m/s, density is 10³ kg/m³ and viscosity is 10⁻³ Pa · s.

Force type	Force order
<u>Electrical force</u> Brownian force	10 ⁵
<u>Attractive force</u> Brownian force	1
<u>Viscous force</u> Brownian force	1
<u>Gravitational force</u> Brownian force	10 ⁻¹
<u>Internal force</u> Brownian force	10 ⁻⁶

Source: Adapted from Russel et al. 1989

2.2 The Non-perfect Image Effect

There are some effects leading to the lower image quality, such as paging time and remnant direct current (RDC). These two effects cause the particles moving to the wrong place and showing the wrong reflectivity. The main reason is the different internal force and initial position. If every time EPD is driven in the dissimilar environments, the reflectivity would not be the same with typical driving waveforms.

2.2.1 Paging Time

When we read a book, the image stays constant for a long time, and the time interval of switching each pages is called paging time. Paging time could be regarded as the stage for ion recombination. When voltage off, the particle should keep the original position. However the internal electric field would force particles and ions to the lowest potential state, so the movement happens [30]. Consequently, the next time when we switch the pages, the internal force and position of the particles are not the same as shown in Fig. 2-6, depending on the paging time. And this effect affects the image quality greatly.

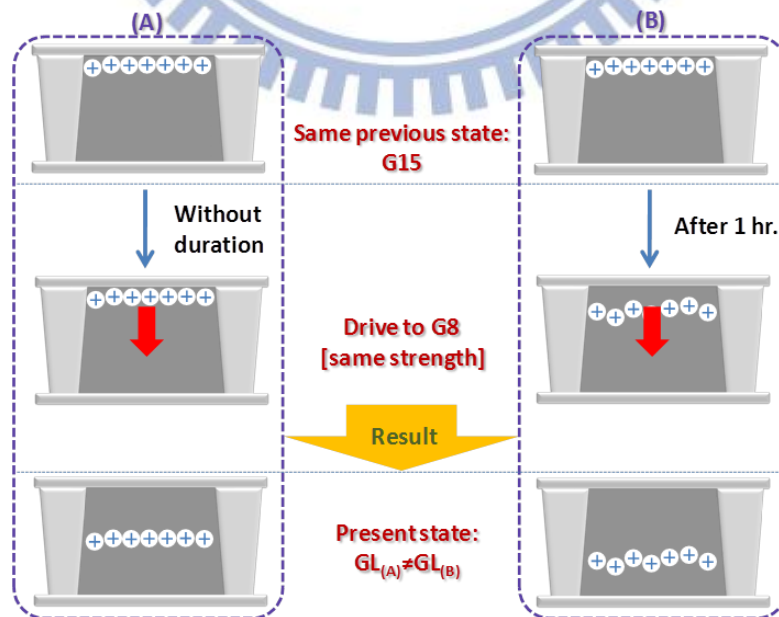


Fig. 2-6 Schematic showing paging time effect.

Due to this effect, the driving waveform usually does a reset process for a same initial state. With the reset process, the image could be displayed the same after different paging time. However, the reset process takes a lot of time and sometimes follows the flicking effect which causes people uncomfortable. Therefore, how to eliminate the paging time effect or optimize the reset process has been an important job in this research field.

2.2.2 The Remnant DC

According to the importance of the internal field, the remnant direct current must play a significant role in the EPD system. When applying voltage, the dielectric material is polarized and forms the dipole. Until the voltage turned off, the dipole creates an internal force to move the particle as shown in Fig. 2-7 and affects the reflectivity. Moreover, switching the image moves not only the particles but also the ions. Therefore, the direct current would induce the dipoles and separate ions to the opposite sides and form the internal electric field too.

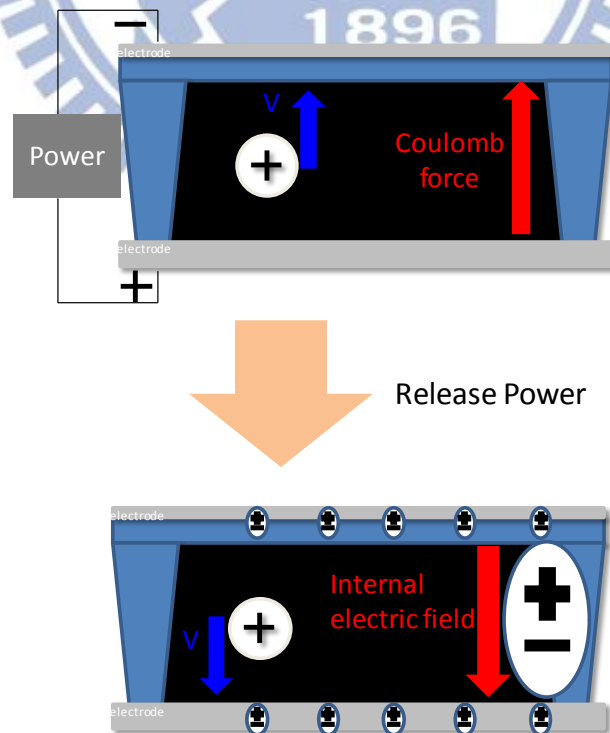
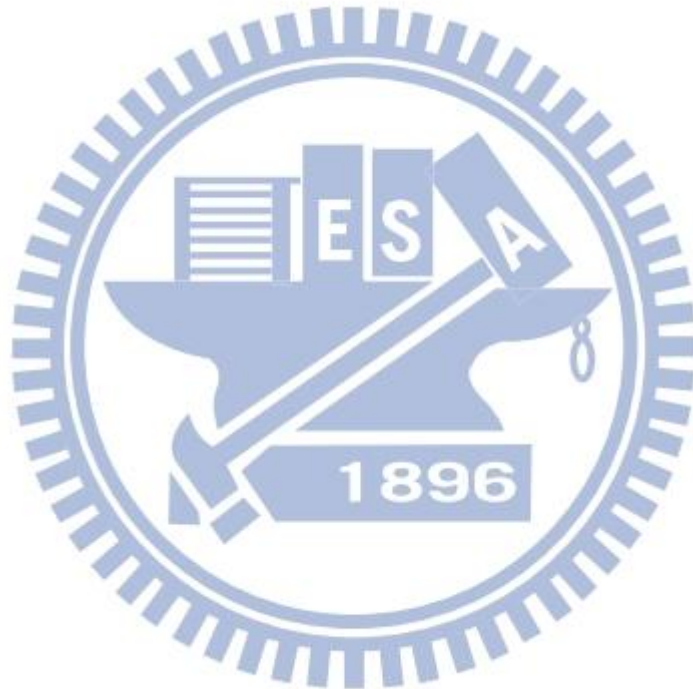


Fig. 2-7 Schematic showing remnant DC effect.

Because of this effect, the driving waveform must add some alternating current pulse to combine the ions or relax the dipoles. For the better quality, the DC balance waveform must be needed to further reduce the remnant DC. Nevertheless, the driving waveform would become longer. Therefore, the lateral driving method might be the solution without remnant DC in shorter waveforms.



Chapter 3. Equipment & Method

In the EPDs measurement, the optical response is the most intuitional for the image quality. Moreover, the microscopic transportation phenomenon is also the thing that we want to understand. So, some equipment and method were needed to get that information.

Photo detection system and microscope system were needed for all optical response not only macroscopic but also microscopic observations. The microscopic lateral observation was needed to get information of particle moving speed, particle packing contrast, and stability in the cell for the transportation phenomenon.

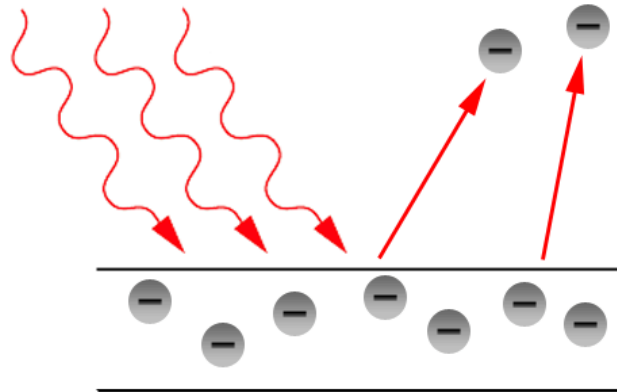
3.1 Equipments

3.1.1 Photo Diode

The optical response was measured by photo diode which worked by photoelectric reaction. Einstein explained the photoelectric effect in A.D. 1887, which occurred because photons collided with electrons and brought up current. The formula was described as shown in Eq.(7), where h is Plunk constant, ν is frequency, ϕ is work function of the material, e is electron charge, and V is voltage of the electron.

It meant that when high energy photon stroke material, the electron in the material would be dissociated with potential eV and absorbed the photon one-on-one as shown in Fig. 3-1. Therefore, in the suitable frequency, the higher reflectivity caused the higher current. In our case, the photo diode which is manufactured by THORLABS Inc. with model number of PDA100A was used for visible light as shown in Fig. 3-2. This photo diode's active areas has 9.8 mm diameter for enough signal in the Lambertian reflectance and also the detection wavelength is 350 to 1100 nm including visible light.

$$h\nu = \phi + eV \quad (7)$$



http://en.wikipedia.org/wiki/File:Photoelectric_effect.png

Fig. 3-1 The photoelectric effect.



Fig. 3-2 The PDA100A photo diode.

3.1.2 Photometer

To prevent the drawback of the photo diode, only the relative signal it showed, the photometer was needed for the luminance information. I-one was chosen for the CIE-Lab measurement and purchased from HomDa Automation Co., Ltd. shown in Fig. 3-3. I-one has the 3.5 mm² active area and 200 Hz scan rate for the experiments, and it can measure not only lightness but also colorimetry. Lightness is the linear feeling of light for human.



http://www.getop.com/upload_image/news_news/59/X-Rite%201%20Pro.jpg

Fig. 3-3 The Photometer, I-one.

3.1.3 Function Generator

During the experiments, the waveform which drove the film was generated by the function generator. The Agilent 33210A with option 001 as shown in Fig. 3-4 was used for the synchronized waveform to each electrodes and the common electrode. The way to synchronize two function generators was connecting them to the time base. If two function generators were connected, the master time base could be the time base output from one of the generator.



Fig. 3-4 The Agilent 33210A function generator.

This function generator can build up the arbitrary waveform which the experiments needed. Putting waveforms into the EPD film, the characteristics were shown and the quality of EPD would be further improved.

3.1.4 Laser Scanning Confocal Microscope

In microscopic observation, microscope was needed. The Olympus IX71 laser scanning fluorescent confocal microscope as shown in Fig. 3-5 was used for the microscopic optical and particle movement understanding.

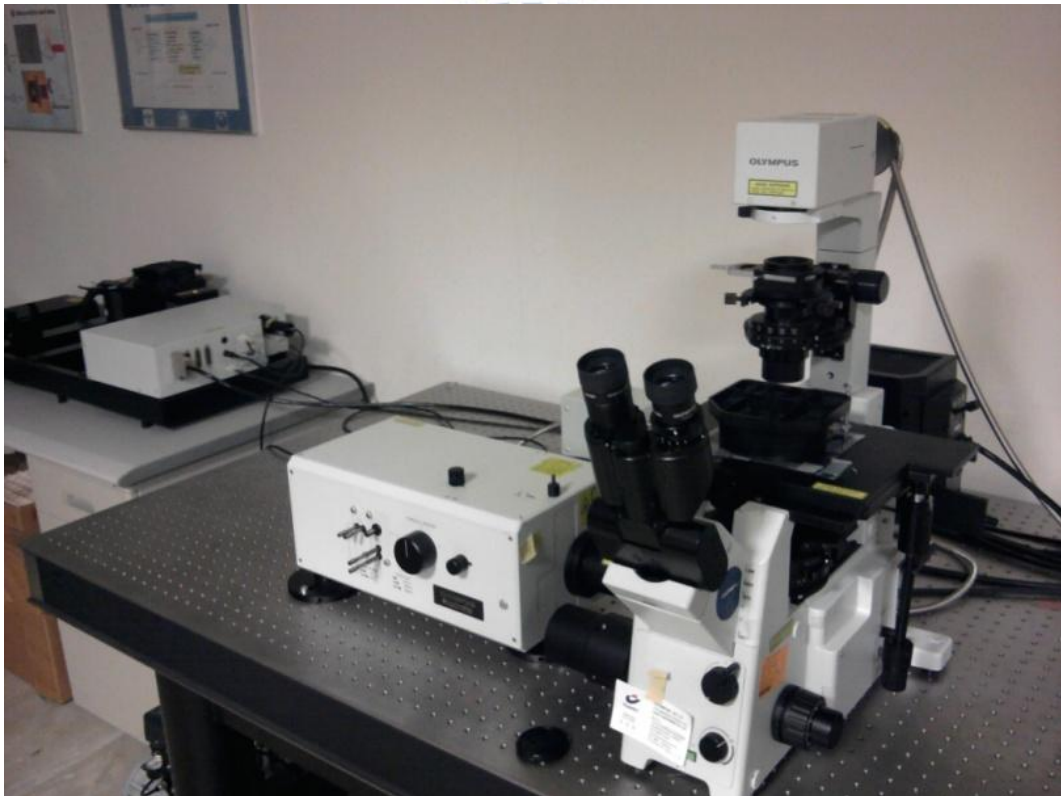


Fig. 3-5 The IX71 laser scanning confocal microscope.

It contains transmissive mode, reflective mode, and laser scanning mode. Transmissive mode was used for the interval of the particles detection; the interval of the particles was distinguished by the light source of haloids lamp forming the higher color saturation. Reflective mode was used for the white and black particles detection, the mercury lamp was the light source emitting white light to discriminate opposite charged particles. Laser

scanning mode operated laser to be light source for the much higher resolution and the function of confocal showed the focal plane image only. All of the modes resolution were higher than 1 μm for the electrophoretic particles.

3.2 Observation System

3.2.1 The Macroscopic System Setup

The 5mW and 632.8 nm wavelength He-Ne laser was set to be the light source and reflected by EPD film. The relative optical response was measured by photo diode as shown in Fig. 3-6, and the absolute lightness value was measured by photometer: I-one [31].

When the different waveforms were put into the EPD film, the instantaneous optical response and the stability of the reflectivity were measured. It was helpful to fine tune the waveform and find out the inadequate part.

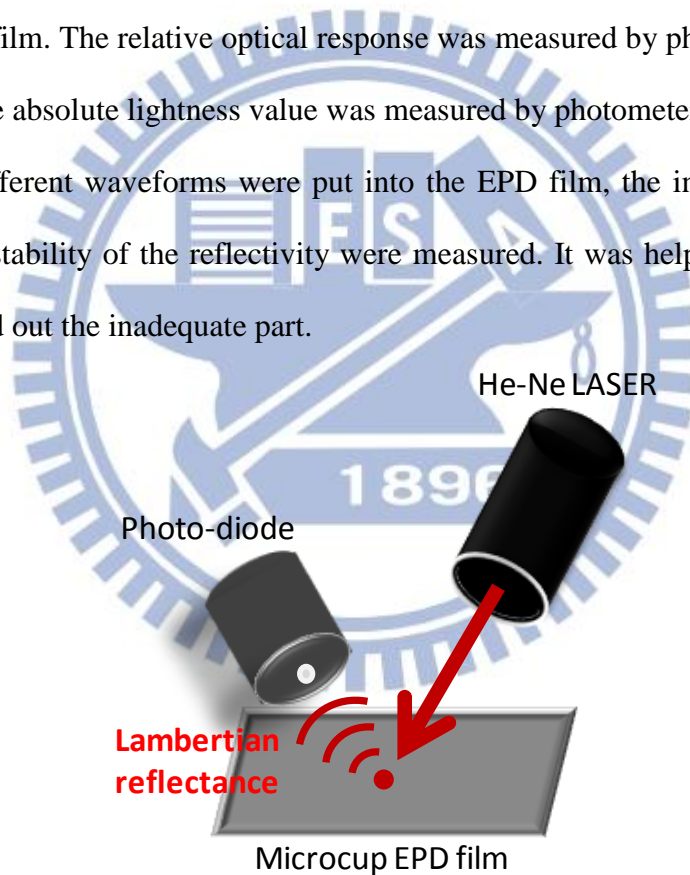


Fig. 3-6 The light path in macroscopic system.

3.2.2 The Microscopic System Setup

Moreover, microscopic system was operated for tiny disparity which was hard to be seen. The microscopic system, including two modes of reflective and transmissive, was set

up to observe the motion of particles inside an EPD, as shown in Fig. 3-7. The optical microscope was operated in the reflective mode to distinguish the luminance states of gray level 0 and gray level 15, respectively.

The optical transmissive mode was used for distinguishing the low concentration part of white and black particles which meant only few particles there. The images were captured instantaneously by a digital video camcorder. Then, three important indexes, including particle moving speed, particle packing contrast, and lateral bistability were introduced to the efficiency of lateral electric field intensity and the stability of the particles. The driving quality was evaluated by these three parameters, and what happened to waveforms in the experiments was found out.

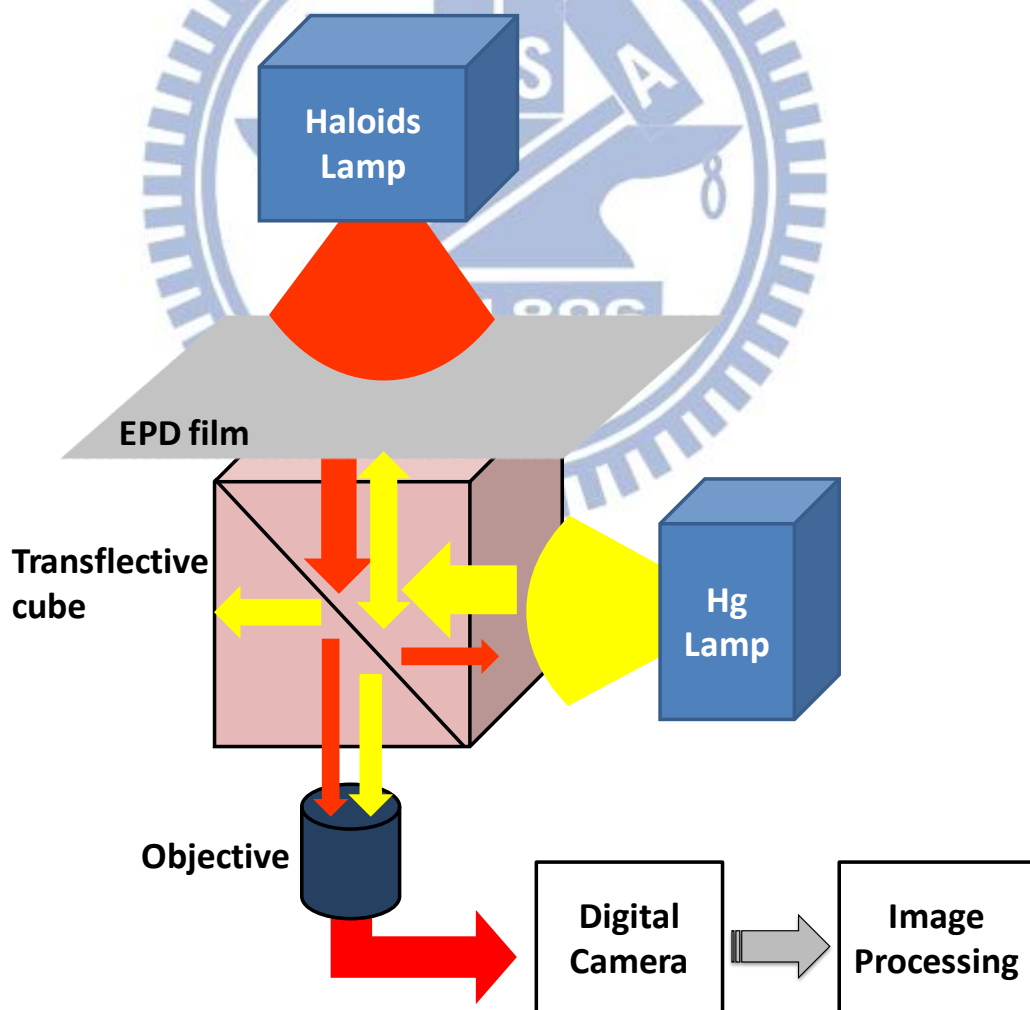


Fig. 3-7 The light path of the microscope system.

The digital image processing used HSL (Hue, Saturation, and Lightness) color space to build the different regions which were white particles, black particles, and few particles in MATLAB programming calculations. The algorithm was shown as shown in Fig. 3-8. The region without particles was deselected by higher saturation light because the haloids lamp light would transmit directly. The gray levels were distinguished by the light intensity. Therefore, the particles distribution could be recognized and analyzed.

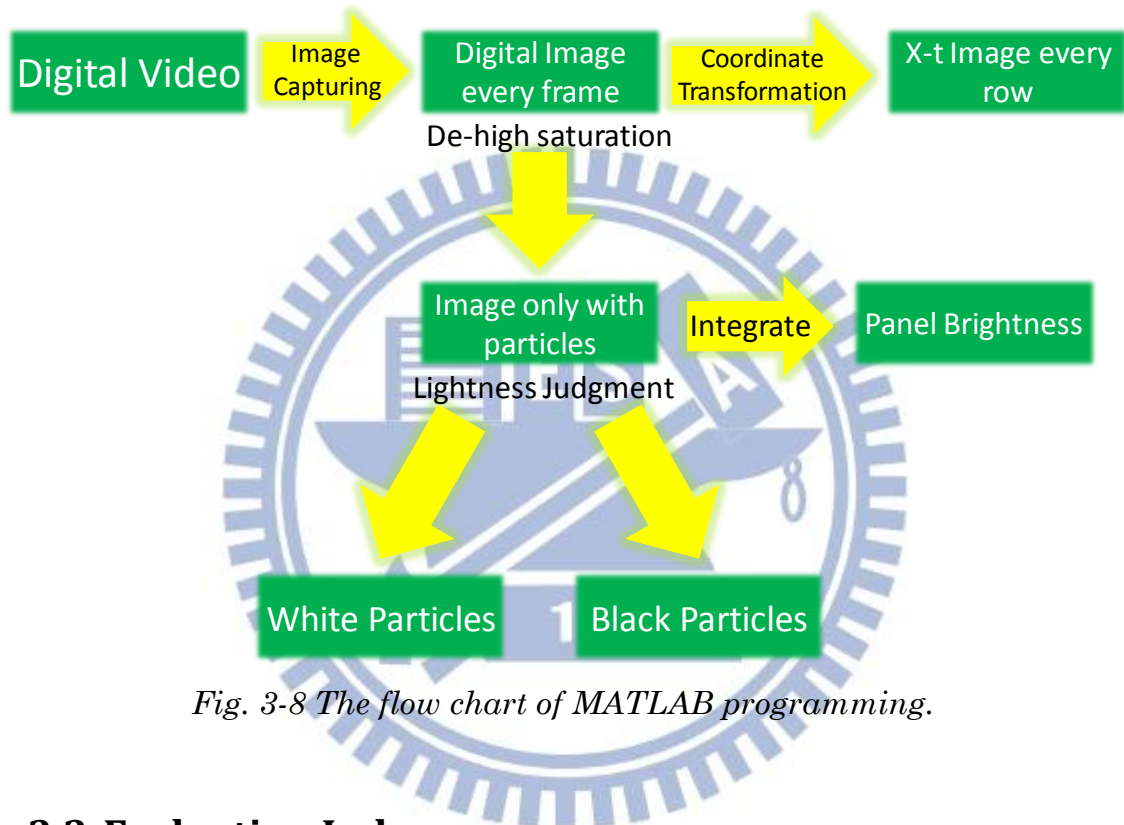


Fig. 3-8 The flow chart of MATLAB programming.

3.3 Evaluation Indexes

There were three parameters for analyzing the experimental results. These parameters were: moving velocity, particle packing contrast, and lateral bistability. These three parameters could be compared to obtain those basic test waveforms' driving advantages, and then we combined those advantages by adding the basic waveform in the driving waveform at the suitable position. The objective was to design the fast response and high contrast ratio driving waveform in the normal direction by observing the phenomena in lateral direction. It might improve the performance logically and physically.

3.3.1 Particle moving velocity $v(t)$

Particle moving speed, $v(t)$, was proportional to the electric field in lateral direction. $v(t)$ was utilized to estimate whether the electrode design had enough electric field along the lateral direction. Particle position of time, $x(t)$, was acquired by analyzing from the video recorder. Deriving $x(t)$, $v(t)$ was got to determine the magnitude of the lateral electric field, as shown in Fig. 3-9.

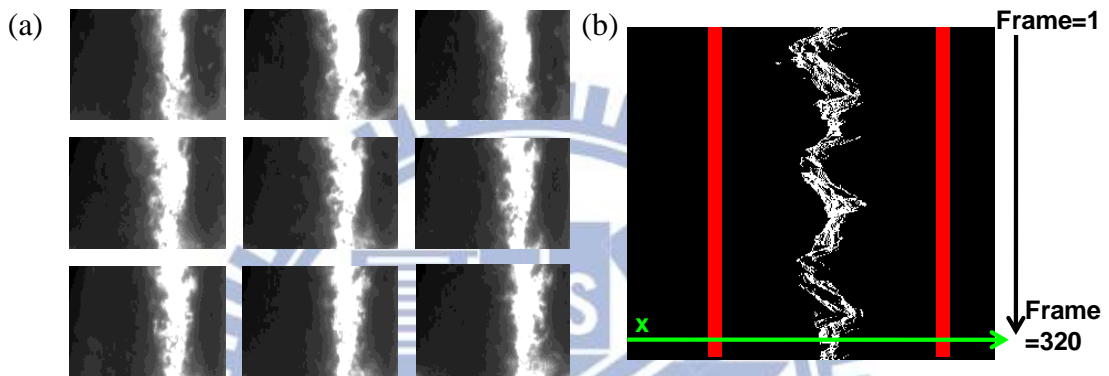


Fig. 3-9 (a) The top view of the video was picked up frame by frame in transmissive mode. (b) The white track was the particle motion in different time along X direction.

3.3.2 Particle Packing Contrast

Particle packing contrast meant that particles were pushed together by a lateral electric field. The stronger the effective lateral electric field was, the more intensive the particle position was. We used image processing to get this parameter as shown in Fig. 3-10(a).

It had low concentration in area A, and high concentration in B. Summing these two area and dividing A by B meant the lateral electric field efficiency to drive those particles in Eq.(8), where A_A and A_B denotes the space at a point in area A and B respectively. When driving voltage was the same, the higher the particle packing contrast was, the larger the lateral driving strength was.

$$Particle\ Packing\ Contrast = \frac{\sum_i A_{A_i}}{\sum_j A_{B_j}} \quad (8)$$

3.3.3 Lateral Bistability (Repulsing speed)

The third factor was bistability in lateral direction. The image stability of EPDs without continuously applying a voltage made it suitable for E-papers. The reflectance remained when particles stopped moving, and the reflectance changed when particles moved. Therefore, the summation of the normalized luminance deviation at each point in the screen when the applied voltage was removed meant the bistability lost as shown in Fig. 3-10(b). Because bistability lost was time dependent, we divided it by time as the repulsing speed in Eq.(9), where ΔY and Δt denotes the deviation of the luminance at each point except the few particles area and the time between two frames respectively.

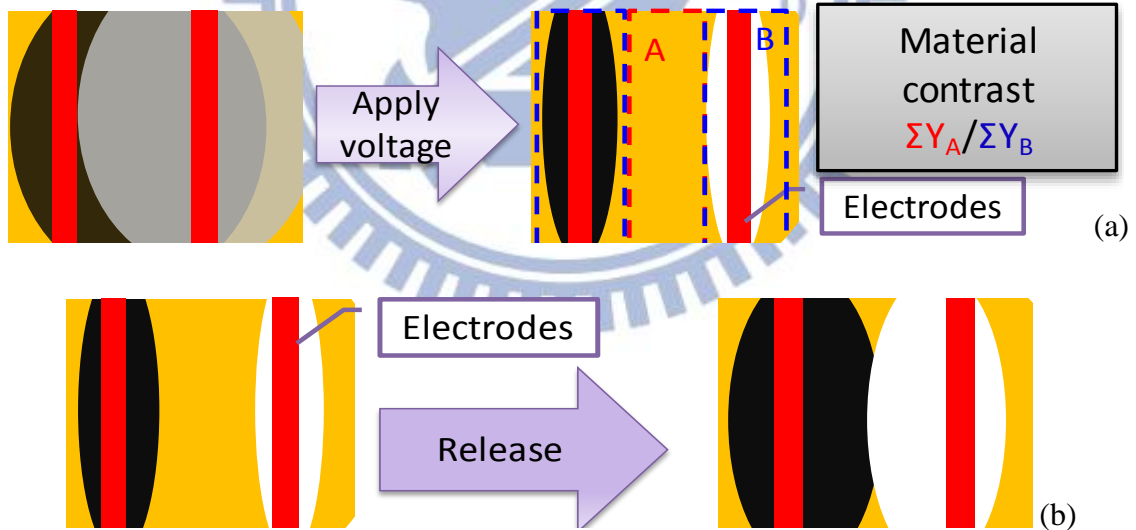


Fig. 3-10 The top view of the cell. Black and white area has high concentration of black and white particles respectively. Yellow area has few particles.

$$Replusing\ Speed = \frac{\sum_i \Delta Y_i}{\Delta t} \quad (9)$$

Chapter 4. Simulations

4.1 Simulation Tool

Before making the electrode for the lateral operation, the simulation process must have been done for better experimental results. COMSOL Multi-physics engineering simulation software was used and its environment facilitated all steps in the modeling process such as defining geometry, meshing, specifying physics, solving, and then visualizing the results. Most of all, this software could simulate not only electrical but also mechanical properties.

The simulation needed only five processes to be completed. First, draw the geometry structures in two or three dimension in the CAD interface. Second, select the physics model. Third, set the material properties in database. Fourth, build the boundary conditions. Finally, run the program and the results would be given.

The boundary condition of electromagnetic was based on Maxwell's equation and the initial value of electric potential was zero. The boundary condition of electrokinetic was based on laminar flow for electrophoretic system and the initial value of velocity was zero. The parameters of the material were set: all the electrodes were made in ITO; the electrophoretic system was set in a low mobility, high relative permittivity and non-polar environment; moreover, the left and right boundaries were set as open boundary to form the infinitely repeatable situation.

4.2 Simulation for Electric Field Distribution

Different widths and pitches of lateral electrodes were simulated to optimize the electric field intensity along the lateral direction before making the real electrode. In-plane electrodes contributed to not only horizontal but also vertical electric field. Therefore, a working ratio was defined as the working area divided by total area, where the working area meant the area when the electric field of X-Y plane was ten times larger than that of Z direction to represent the percentage of electric field along the lateral direction as shown in Fig. 4-1.

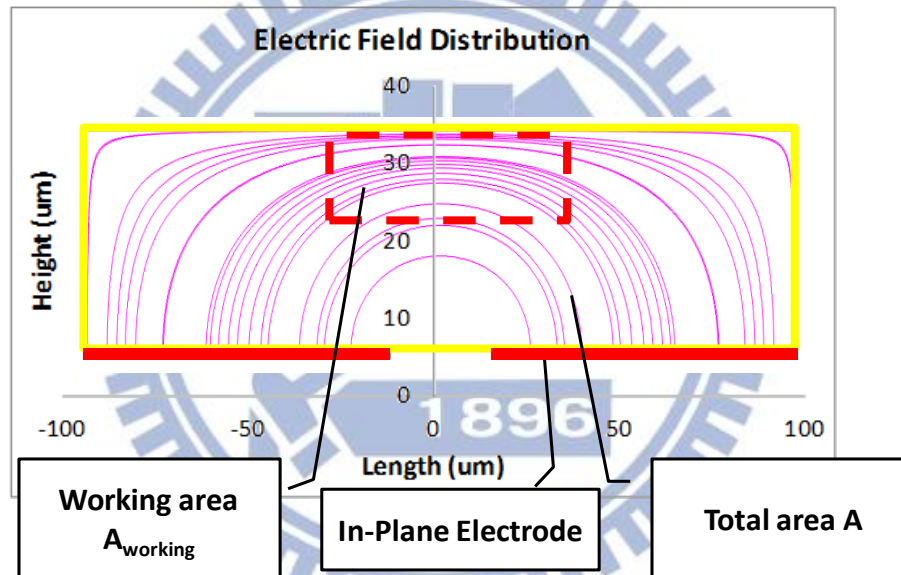


Fig. 4-1. The cross section of electric distribution in the cell, working ratio is defined as $A_{working}$ (red dashed square)/ A (yellow solid square).

In the simulation results, when the pitch between two electrodes (L) was fixed at 100 μm , smaller electrode width (W) would get larger lateral electric field and working ratio, as shown in Fig. 4-2(a). On the other hand, with the same W , 50 μm , the longer the L was, the smaller the electric field and the larger the working ratio was, as shown in Fig. 4-2(b). According to the results, we knew that better electrode design should be small W with a proper L for large enough electric field intensity and working ratio in the lateral direction.

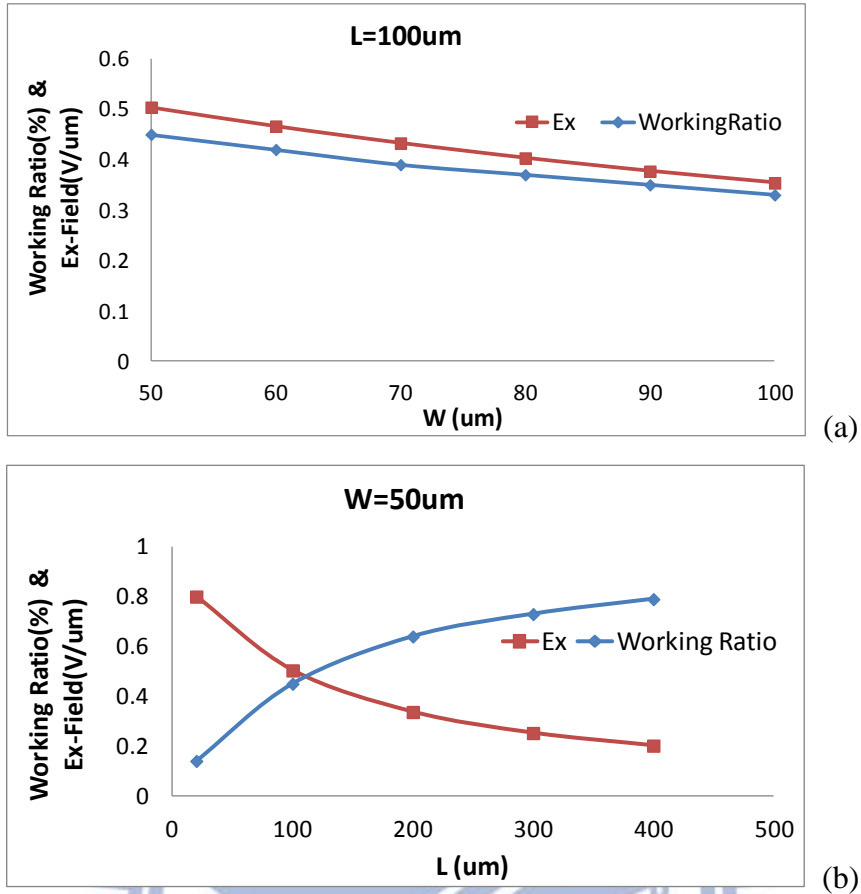


Fig. 4-2 (a) The conditions with L fixed at 100 μm . (b) W fixed at 50 μm . Red curves are electric field along the lateral direction. Blue ones are working ratio.

Considering the lateral electric field intensity and working ratio, the electrode size of $W = 50 \mu\text{m}$ and $L = 200 \mu\text{m}$ was chosen and shown in Fig. 4-3. In this size, working ratio was larger than 50 % and the lateral electric field was larger than 0.3 V/ μm in 60 V. This driving voltage of 60 V was also the largest applied voltage for the following experiments.

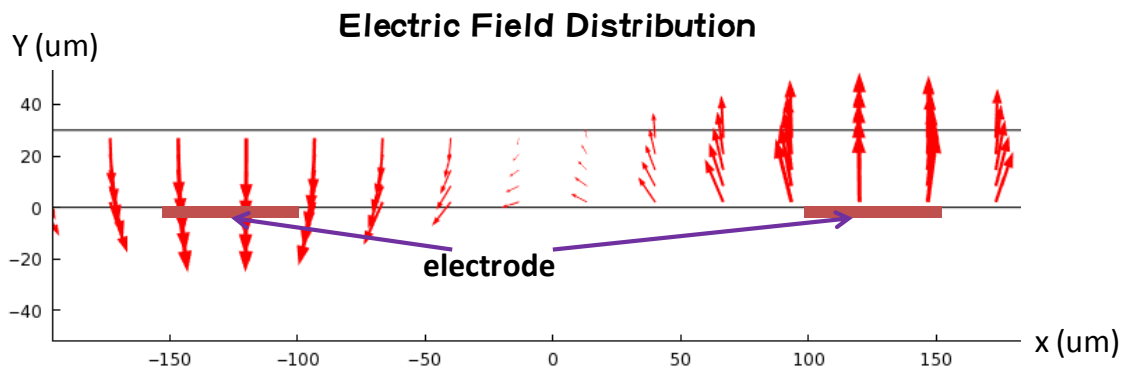


Fig. 4-3 The electric field distribution in $W = 50 \mu\text{m}$ $L = 200 \mu\text{m}$ lateral operation.

4.3 Simulation for Hydromechanics

After electric field was simulated, the hydromechanics should be simulated too for electrophoretic situations. The electrophoresis was affected by both electric field and transport phenomenon, and formed hydrodynamic which was caused by electrical force. Since $W = 50 \mu\text{m}$ and $L = 200 \mu\text{m}$ electrode was chosen in Section 4.2, the hydrodynamical simulation must be done to predict the particles transition and make sure the flow was needed by the displayed images.

The trend of the electrophoresis flow included charged particles, micelles, anti-micelles, and ions. The simulation results were shown below. The velocity field distribution was shown as shown in Fig. 4-4, the lower layer flowed along the electric field and the upper layer flowed along the opposite direction of electric field. The velocity distribution which meant the absolute value of velocity was shown as shown in Fig. 4-5. The lower layer had the highest velocity and upper layer had less one. The speed of bottom layer was about four times higher than that of top layer. Therefore, most of the particles in the lower layer swam close to the electrodes. But few upper layers' particles would be carried by the flow to the electrode as well. However, at this tiny speed, the upper layer could not be cleaned in enough time for driving the image. Therefore, changing the image still needed the vertical electric field and lateral one could be the assistant.

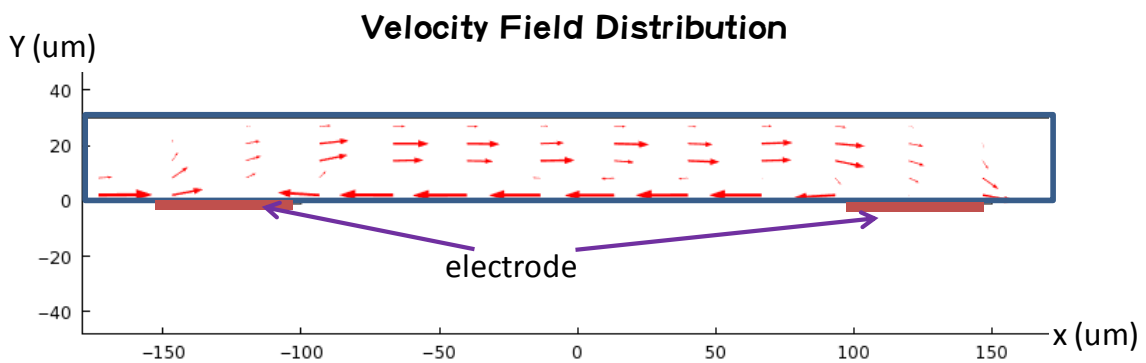


Fig. 4-4 The particle flow in $W = 50 \mu\text{m}$ $L = 200 \mu\text{m}$ lateral operation.

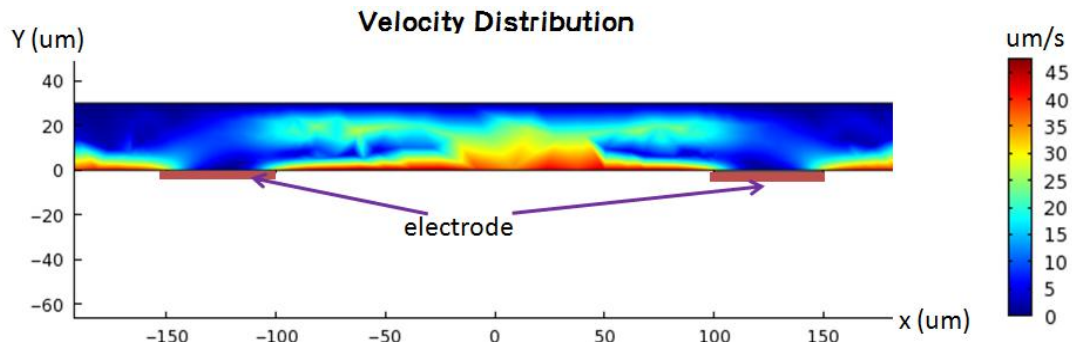


Fig. 4-5 The velocity strength in $W = 50 \mu\text{m}$ $L = 200 \mu\text{m}$ lateral operation.

4.4 Optimization for Real Product Case

In the real case of electrode design, both the working ratio and the electric field should be considered at the same time. The electrode size should be smaller for better experimental results because of the stronger electric field. The electric field should be higher than $0.3 \text{ V}/\mu\text{m}$ at 15 V which was suitable in active matrix. Now the high driving voltage and long driving time in our prototype could not be accepted in the lateral driving.

The simulations for the future electrode design were done in Fig. 4-6, and the best result was $W = 5 \mu\text{m}$ $L = 20 \mu\text{m}$. The smaller the electrode size was, the more expensive the cost was, and the harder the manufacture was. But, the smaller size electrodes could drive not only along vertical direction but also along lateral direction at the same time because of enough density of electrodes and strength of electric field respectively. Therefore, the multi-driving method could be used in the future.

In this case, the electric field got larger in the same driving voltage. The electric field could reach $0.3 \text{ V}/\mu\text{m}$ in 15 volt as same as the vertical electric field. In $\pm 15 \text{ volt}$ driving status, the electric potential distribution was showed in Fig. 4-7, and the gradient of potential was near the electrode at bottom. So the strong electric field formed in the lower layer as shown in Fig. 4-8. The electric field could reach $0.6 \text{ V}/\mu\text{m}$ maximum and $0.3 \text{ V}/\mu\text{m}$ under $5 \mu\text{m}$ depth. Therefore, the highest hydrodynamic was made near the bottom by strong electric field.

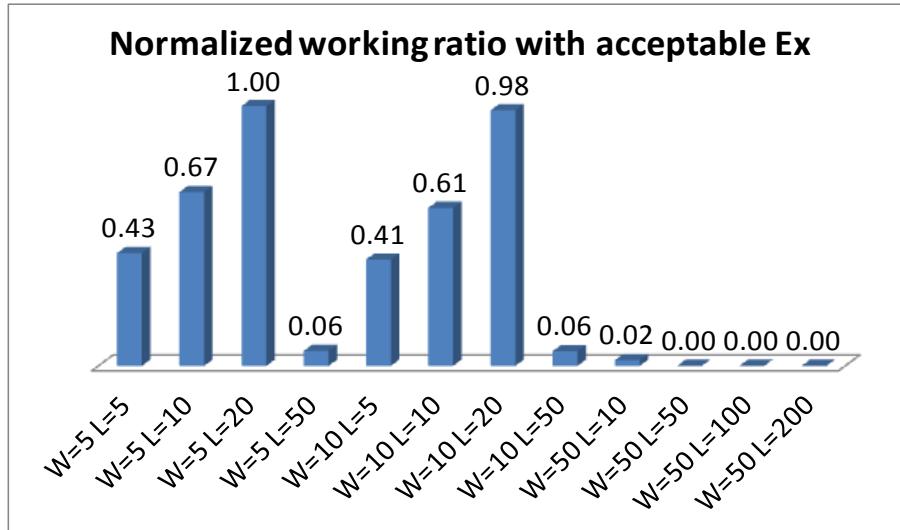


Fig. 4-6 Normalized working ratio with acceptable electric field ($E_x > 0.3 \text{ V}/\mu\text{m}$)

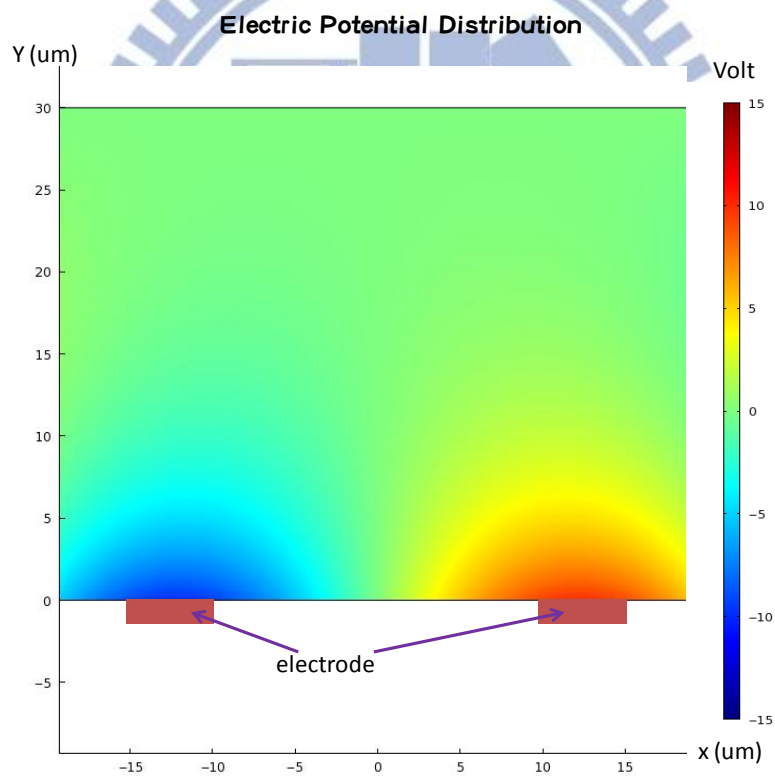


Fig. 4-7 The voltage distribution in $W = 5 \mu\text{m}$ $L = 20 \mu\text{m}$ lateral operation.

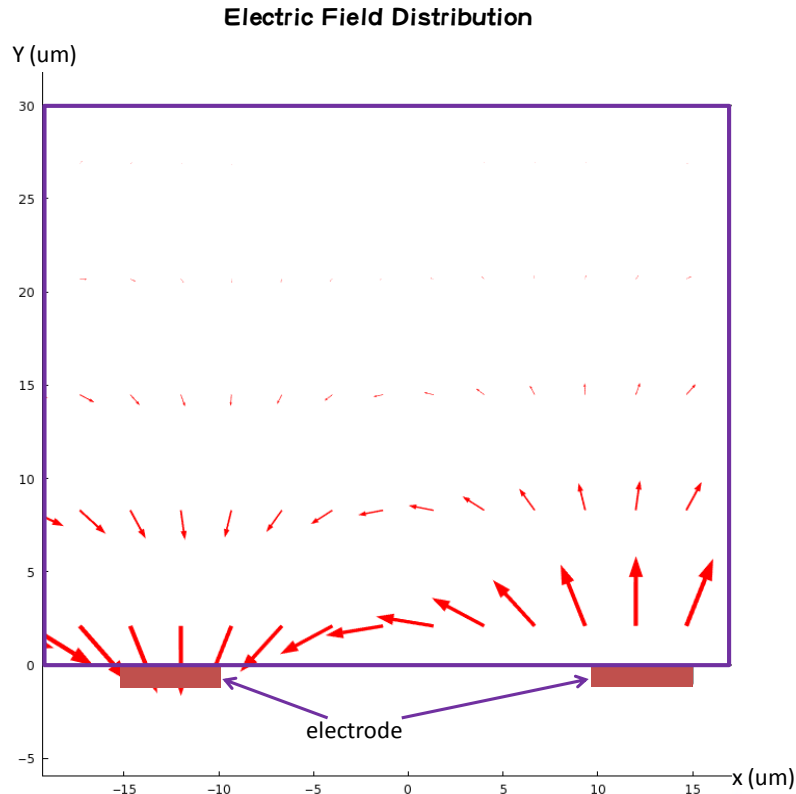


Fig. 4-8 The electric field distribution in $W = 5 \mu\text{m}$ $L = 20 \mu\text{m}$ lateral operation.

In hydromechanics, there were two main laminar flows as the yellow and red region in Fig. 4-9. The flow direction in this two region was opposite as shown in Fig. 4-10. Both two regions had large flow; it carried not only ions but also particles. Fortuitously, the flow speed of bottom layer was twice higher than upper layer. The speed deviation could be used for lateral driving applications. Also, particles could be separated by those driving methods and formed the quality images.

According to the simulation results, the electrodes were fabricated for the experiments. The $W = 50 \mu\text{m}$, $L = 200 \mu\text{m}$ electrodes had the larger size for easy observation. On the other hand, the $W = 5 \mu\text{m}$, $L = 20 \mu\text{m}$ electrodes were fabricated for better applications. However, five micrometer ITO fabrication process was difficult to achieve in our equipment. So the $W = 10 \mu\text{m}$, $L = 20 \mu\text{m}$ and $L = 40 \mu\text{m}$ electrodes were made to replace it. If the smaller electrode width could be made, the better results would be given.

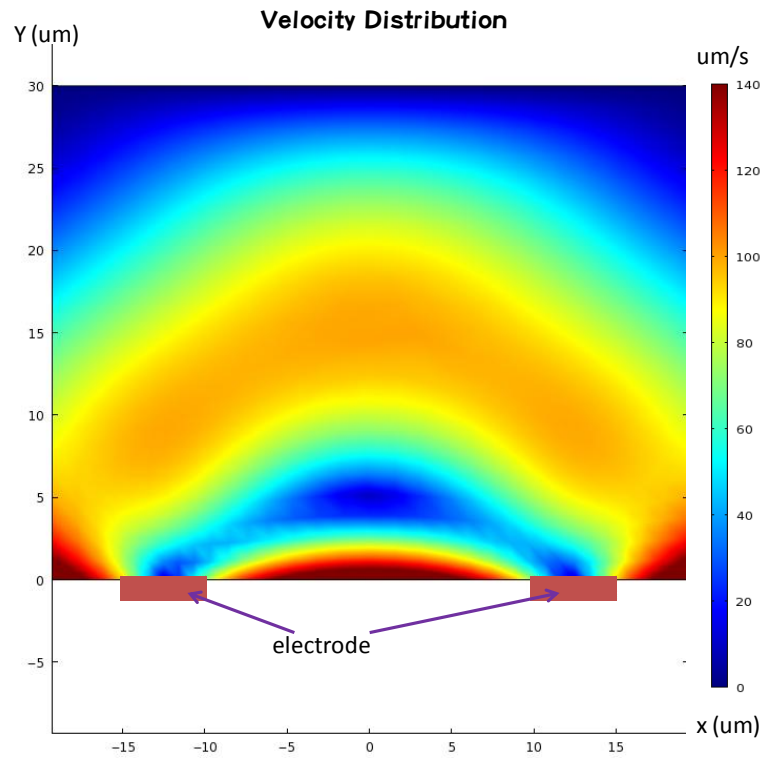


Fig. 4-9 The velocity distribution in $W = 5 \mu\text{m}$ $L = 20 \mu\text{m}$ lateral operation.

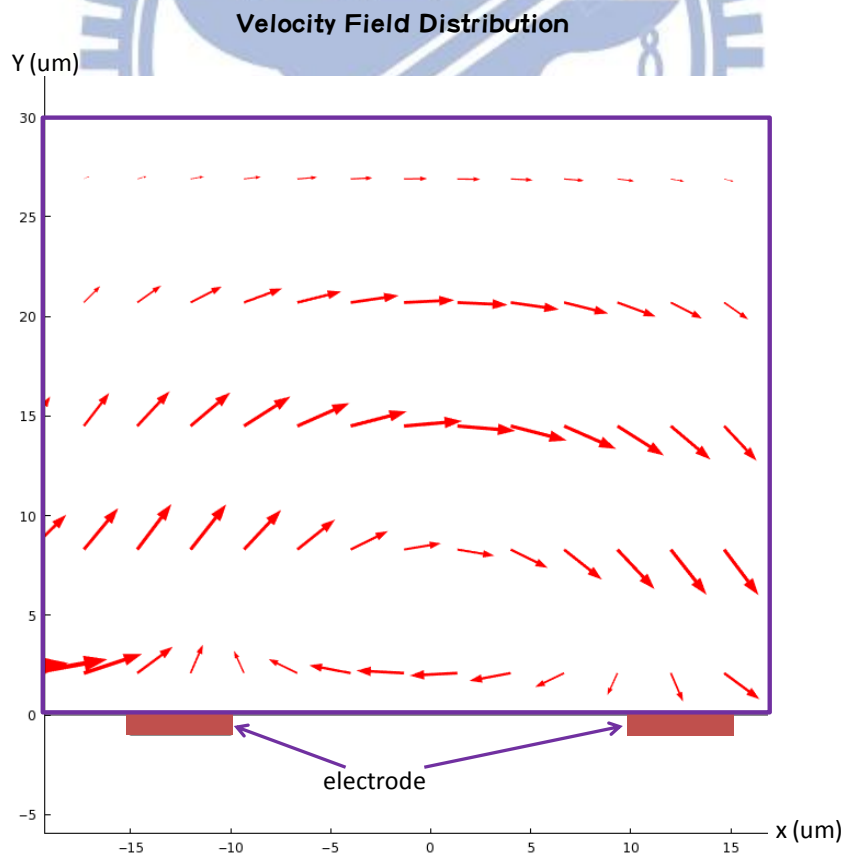


Fig. 4-10 The velocity field distribution in $W = 5 \mu\text{m}$ $L = 20 \mu\text{m}$ lateral operation.

Chapter 5. Experimental Results

5.1 Mechanism Confirmation

To observe the motion of particles, three basic waveforms were chosen: direct current (DC), shaking, and pulsing. In these three driving waveforms, the positive driving period was the same but with different front electric behaviors. DC was just like continuous electric field to drive those particles. Shaking had the reverse bias before the main electric field to neutralize ions [32] which was dissociated when an EPD was driven. And pulsing had a rest before the electric field was applied.

The three test waveforms and the experimental setup are shown in Fig. 5-1. The videos were captured when the waveforms started. Because of the pitch of each two electrodes were larger than the cell gap (approximate 30 μm), the lateral electric field was smaller than conventional vertical one, so that the driving voltage and the driving time were larger. The driving time was chosen 1000 ms for simple driving and 4000 ms for over push driving which meant the particle was still pushed even at the end of the boundary. Moreover, 15V which was less than 0.1 $\text{V}/\mu\text{m}$ was needed for the under threshold situation.

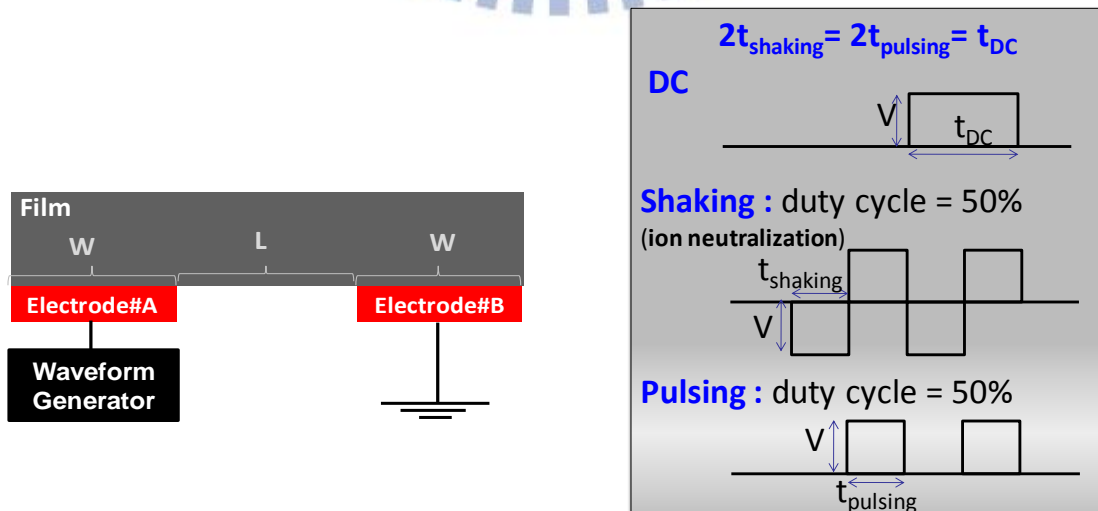


Fig. 5-1 The basic waveforms are DC, shaking, and pulsing.

5.1.1 Experiment of Moving Velocity $v(t)$

When the applied voltage was 15 V, the maximum speed of 4000 ms DC driving (cyan curve) was 300 $\mu\text{m/s}$ and the others were 200 $\mu\text{m/s}$ as shown in Fig. 5-2. The voltage was gained to 30 V, both of the DC and pulsing waveforms' maximum speed were gained to about 570 $\mu\text{m/s}$, but shaking waveform were 300 $\mu\text{m/s}$ and 500 $\mu\text{m/s}$ at 1000 ms (green curve) and 4000 ms (orange curve) driving, respectively. At the largest voltage of this experiment, 60 V, DC and pulsing waveforms' maximum speed were only increased to 680 $\mu\text{m/s}$, and shaking was at 500 $\mu\text{m/s}$. Most of all, in 30 V and 60 V, the pulsing waveform (blue and purple curve) was the fastest at 600 $\mu\text{m/s}$ and 700 $\mu\text{m/s}$, respectively. The possible reason of the nonlinear speed was caused by the other force instead of electrical force in the system.

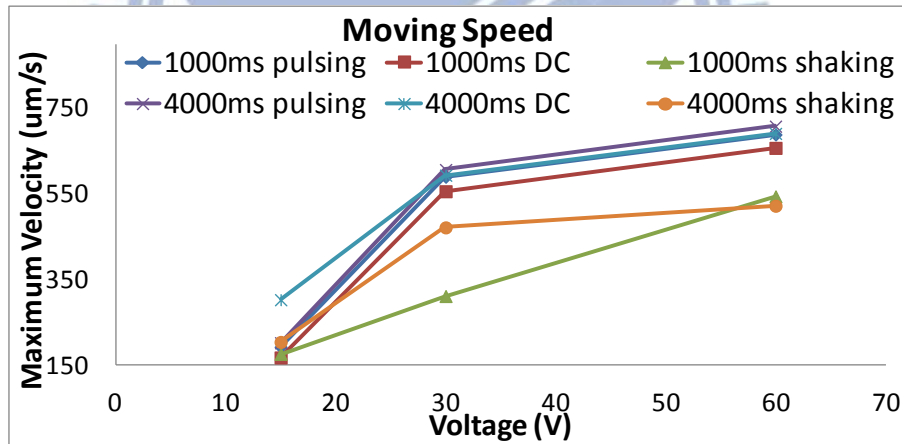


Fig. 5-2 The curves including different driving time and waveforms are plotted as the particles maximum speed.

Particles were accelerated by the total force included applying electrical force, viscosity, internal electrical force which was induced by the ions and charged particles in the cell, and so on. The electrical force dominated the system, and electric field would be increased when applying a larger voltage. However, the moving speed of particles was not double when driving at twice voltage except using 1000 ms shaking. The 1000 ms shaking

waveform (green curve) had the ion neutralized characteristic, with this phenomenon; the velocity was proportional to the voltage. At 15 V, under the threshold [32], the continuous electric field would accelerate particles to higher velocity 300 $\mu\text{m/s}$ still slowly. When the voltage increased over the threshold might destroy the phenomena which brought the threshold. The 60 V pulsing would lead to the acceleration of the particle because the short time rest could recombine ions to reduce the resistible force. However, when the voltage became too high, the effect would be decreased due to the resistant of internal electric field. Therefore, the largest voltage pulsing waveform which was suitable for accelerate to the higher speed in the device could be added before the driving waveform to get much faster speed.

5.1.2 Experiment of Packing Contrast

The particle packing contrast was different in the test waveforms. There were two kinds of the trend, when the voltage increased the particle packing contrast continuous rose or consisted to descend as shown in Fig. 5-3. The particle packing contrast of 4000 ms DC (cyan curve) and pulsing (purple curve) was 9.7 and 7.7 in 15 V respectively; in 30 V, particle packing contrast became to 9.3 and 9.5, finally, 60 V made particle packing contrast decayed to 7.3 and 8.4 in each waveform. The particle packing contrast decreased because the effective force decreased in lateral direction. The resistant force from the internal electric field was carried out by the ions separated in the cell, so the particle packing contrast was not large as the 4000 ms driving time in DC and pulsing. However, the 1000 ms waveforms and 4000 ms shaking (orange curve) did not have this characteristic. Assume that 4000 ms waveforms were in the steady state with the balance force, shaking would neutralize the ion powerfully shown from the 60V 4000 ms shaking waveform had the 11.6 particle packing contrast.

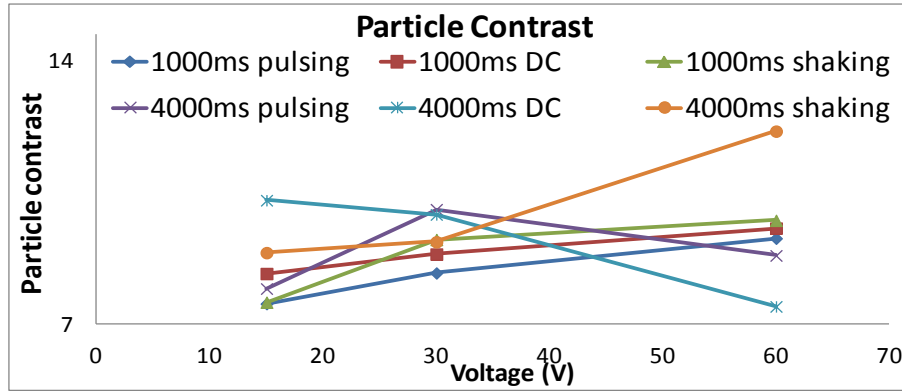


Fig. 5-3 The particle packing contrast versus voltage curves are plotted containing different driving time and waveforms.

Other conditions: without over-pushing, the particle packing contrast raised when the voltage rose in 1000 ms driving time. Under the threshold voltage, 15 V, DC (red curve) still moved the particles strongly; the particle packing contrast was 8. But, when the voltage increased over the threshold, the internal electric field affected particles motion that the particle packing contrast of shaking had to go up to 8.7. Moreover, the highest particle packing contrast was 9.2 in shaking waveform with 60 V, because the internal electric field was further reduced. Therefore, without the process of ion neutralization, the stronger the electric field was, the larger the resistant force was. The driving waveform should avoid the strong resistant force to induced the remnant DC destroyed the balance of the system.

On the other hand, the particles with different packing could display the same gray level because the gray scale generated by mixing the white and black particles and an EPD was a Lambertian system. The loose particle packing contrast could be driven faster owing to the moving distance. As a result, at the end of the driving waveform could be added “short time shaking or pulsing under the threshold voltage” which were chosen for low particle packing contrast in invariable gray level condition.

5.1.3 Experiment of Bistability (Repulsing Speed)

The bistability divided into two kinds of state, short term and long term, was analyzed. The short term and long term bistability was measured after the end of the waveform 10 and 60 seconds, respectively. The repulsing speed was shown in Fig. 5-4, which meant the particle diffused by internal electric field when the voltage was turned off. The continuous electric field or higher voltage would cause the internal electric field strongly which was shown above, so 4000 ms DC (cyan curve) driving in 60 V made the bistability worst no matter short and long terms. For the long term bistability, all of waveforms were about 80 %/s except 4000 ms DC, it might be the particles Brownian motion in the EPD cell. Without the huge resistant force, the long term bistability would be solved from the materials.

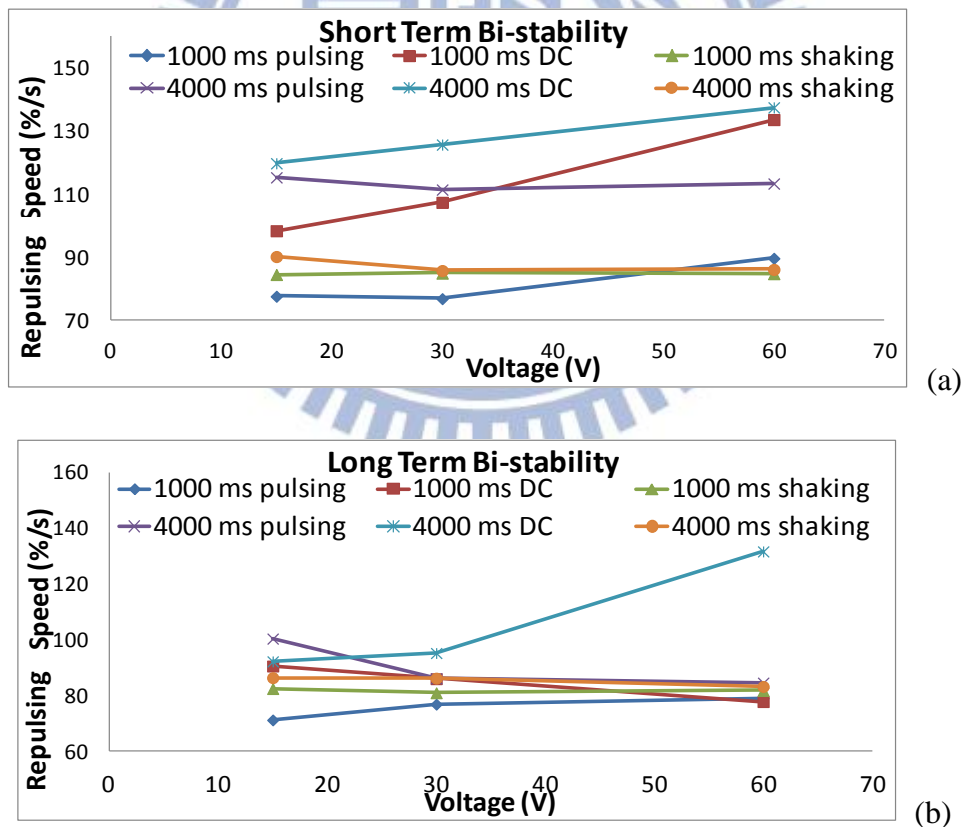


Fig. 5-4 (a) Short term bistability (b) long term bistability including different driving time and waveforms are plotted in versus voltage.

The short term bistability was more important than long term for the comfortable reading experience. The DC driving and 4000 ms pulsing (purple curve) had the bad results, the repulsing speed over than 100 %/s. The remainder of the three waveforms, shaking and 1000 ms pulsing were suitable for driving with good bistability, repulsing speed was less than 90 %/s. Moreover, the 1000 ms pulsing had the repulsing speed less than 80 %/s when voltage under 30 V. But the voltage increased to 60 V, the repulsing speed rose to 90 %/s, so the bistability decreased when the voltage rose. However, the fast response time needed the higher voltage. It seemed to be the tradeoff between speed and bistability. Since the ion neutralization could enhance the stability due to the deficient internal electric field. Shaking waveform could be added after the end of the driving waveform, which let bistability higher than before.

5.1.4 Microcup System Force Model

According to the theory in Chapter 2, the internal forces were induced by the charged ions which were dispersed inside the microcup. The experiments were done in the microcup electrophoresis system, so the force model in this system was built. The model was divided into two main types: stable state and driving state. In stable state, it was also divided into two classifications: long term and short term. The dominant forces were different in each step.

To leave aside Brownian's motions, the neutralized electrophoretic display had force balance between gravity force and viscosity force initially. When electric field was applied, it carried external electric force to accelerate charged materials and electric double layer was dragged to form the opposite electric force to each particle as shown in Fig. 5-5. Then, the internal electric force was caused by charged particles and ions separation. Including another obstructive force, the larger the particle speed was the larger the viscosity force was. Finally, particles stopped beside the electrodes because there was little lateral electric force,

and the particle speed was not big enough to defeat the resistant force. Therefore, particles kept balance with one another by the van der Waal force and formed the screening field to repulse the other particles as shown in Fig. 5-6.

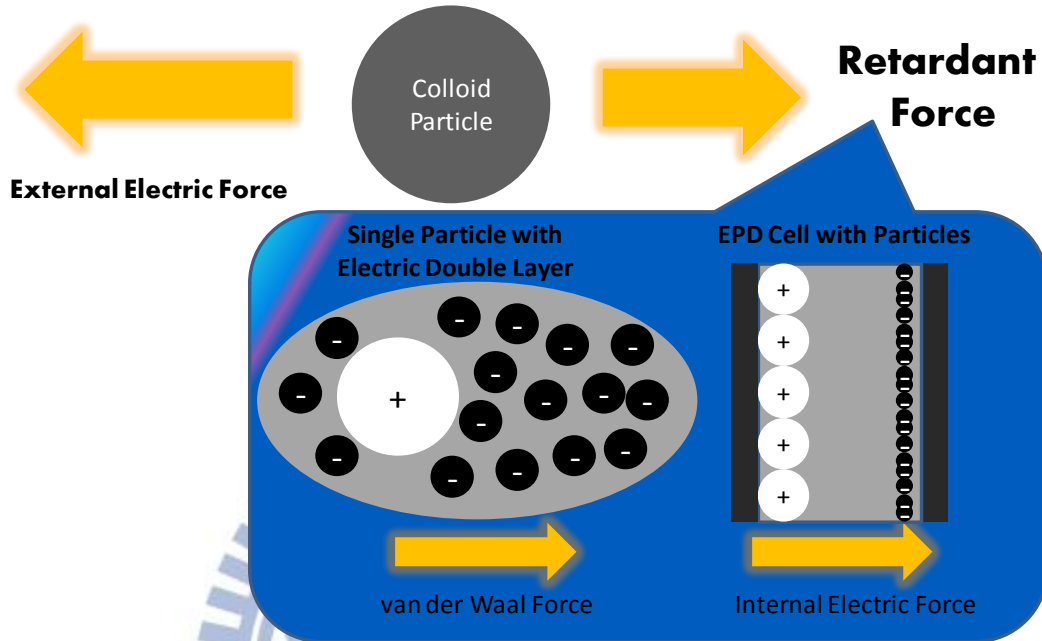


Fig. 5-5 The forces happened when diving.

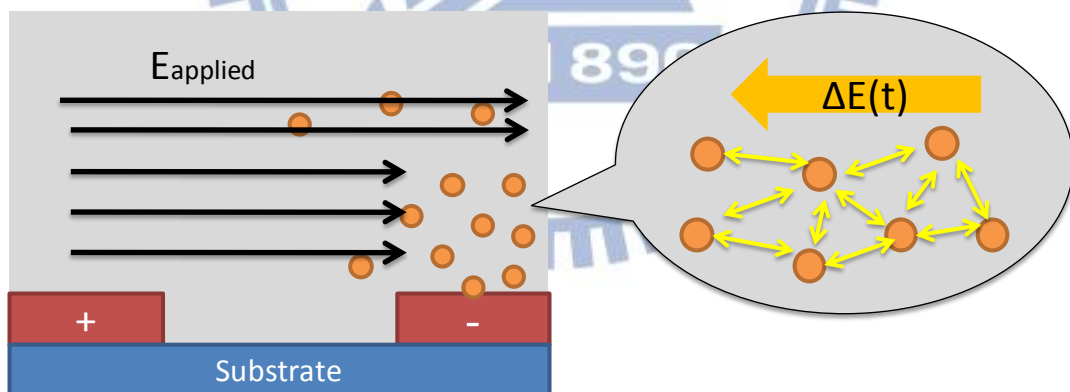


Fig. 5-6 The screening field caused the repulsive electric field.

On the other hand, in the stable state internal electric force still remained due to the separable charged particles and ions. However, in this state voltage was not applied to induce external electric field, so particles would be pushed by the internal force and the reflectivity would be changed. For long term, particles and ions were attracted by the different polarization until the ions were neutralized, so that the internal electric force

became weak. Finally, the particles just swam in Brownian's motion, and reflectivity was kept the same by the isotropic and homogeneous particle motion as shown in Fig. 5-7.

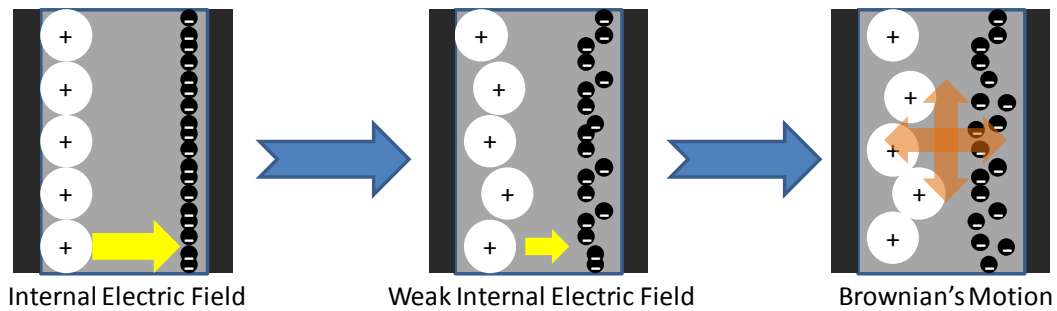


Fig. 5-7 The stable state force evolution.

Consequently, the electrophoretic display force model was built. It would be helpful for the driving method which could reach high image quality and fast particle transition. For the particles transition, the retardant force should be minimized. For the image quality, the ion neutralization should be done before the target reflectivity was achieved for the bistability, and the particles should be transported at the lowest internal electric field for the particles packing consistency. Therefore, the high performance EPD would be developed.

5.1.5 Correlation with Lateral and Vertical

In this part, vertical phenomena by observing the particles motions in lateral direction were confirmed. Because the bistability lost was always affected by the Brownian's motion, the repulsing happens no matter in the lateral or vertical direction. Therefore, the extreme white and extreme black could not last for a long time. But when the interspaces became stable, the darker white or brighter black can be displayed as long as needed.

In vertical direction, when higher voltage was applied, the whiteness could not get higher but the response was fast as shown in Fig. 5-8. The 10 V driving reached 190 mV in 800 ms, the 12.5 V driving used 500 ms to get 180 mV, and the 15V driving changed to 180 mV in 400 ms. Moreover, the slope of optical response was different in first step but approached to others later.

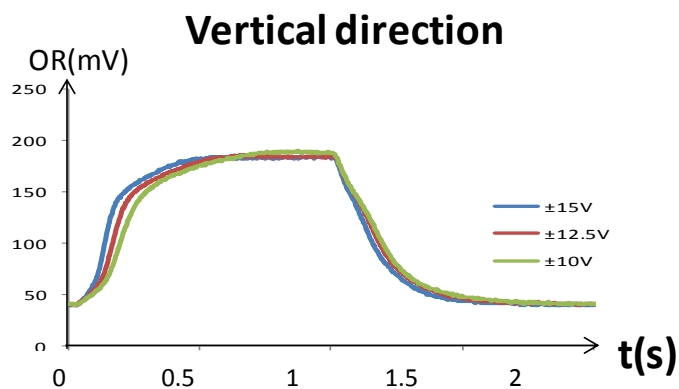


Fig. 5-8 The optical responses in different voltage at vertical direction.

But in lateral direction, the higher voltage caused the higher particle packing contrast. Because the optical response was dominated by mixing the different reflectivity particles, the gray levels were displayed by particles mixing, as the expected model shown in Fig. 5-9(a). As the result, the degree of particle concentration did not dominate the gray levels. Unexpectedly, small voltage could reach higher contrast ratio. The reason was that particles applied to smaller voltage flowed slower and the retardant force was small, so the detachment of particle was higher. In this way, we could get purer particles in different sites as shown in Fig. 5-9(b).

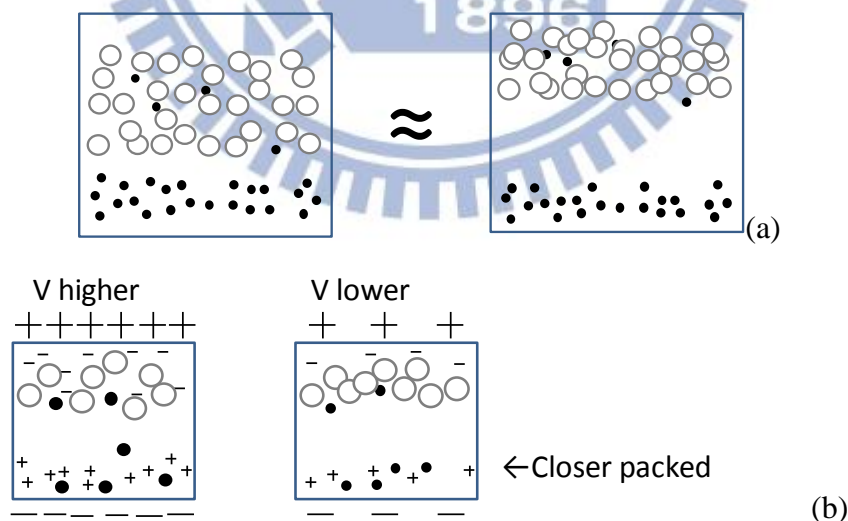


Fig. 5-9 The expected model forms the gray levels with white and black particle.

(a) The optical response was not dominated by the concentration of the particles.

(b) Different voltage packed the different purity of particles.

5.2 Application Proposition

In application part, W would change to 10 μm and L would change to 20 μm for larger electric field. The lateral driving methods which could be used in the electrophoresis system was proposed. There were two channels in the same pixel, so the electric field had higher degree of freedom. The electric force could drive particles or ions in lateral and vertical direction. By doing so, the image quality and response time would be enhanced.

The experimental setup was shown in Fig. 5-10; the signals were applied to the different electrodes at the same time. This method could contribute to no matter lateral or vertical electric field to move the particles as the designer desired. To build up the lateral electric field, the signals #1 and #2 were opposite polarity. Similarly, when the signal #1 and #2 were the same polarity, the vertical electric field was built up. Therefore, lateral driving method could be used for the higher driving degree of freedom.

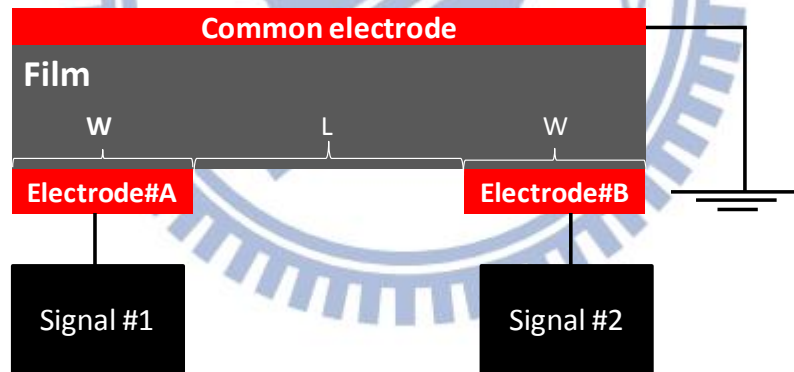


Fig. 5-10 The lateral driving method setup.

The three-step driving method was proposed. Commonly, the driving method was two steps including reset and image driving phase. In lateral driving, it could use three steps driving method for better image quality and response time. The first two steps was reset which used the lateral electric field mainly to prevent flicking effect. The third step was driving which used the mixed electric field to contribute not only vertical but also lateral electric fields.

5.2.1 Lateral Reset

The lateral reset waveform was just like vertical reset including shaking and forming the extreme state. In this waveform, the lateral electric field affected only near bottom layer's particles, so the reflectivity was not changed heavily. The waveform was described as shown in Fig. 5-11. In phase one, lateral shaking recombined the slight-massed ions quickly, even though the electric field was tiny, it could push those ions easily. In the second phase, lateral separation pushed bottom layer's particles to the electrodes for stronger electric field in the driving phase and prevented particles collision as shown in Fig. 5-12.

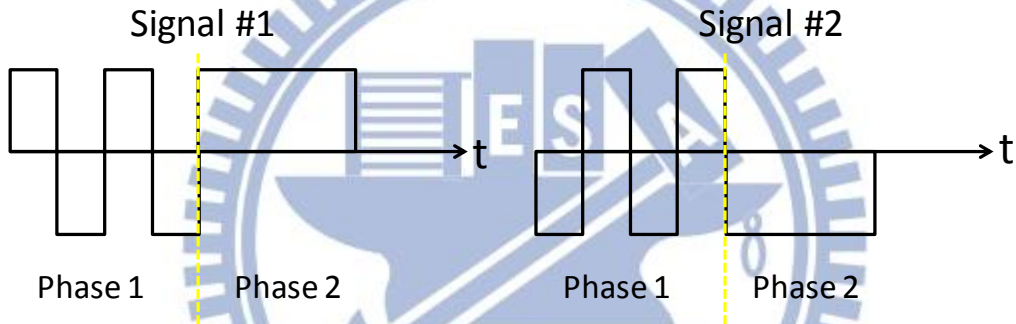


Fig. 5-11 The lateral reset waveform by the opposite polarity in signal 1 and 2.

Non-collided transition

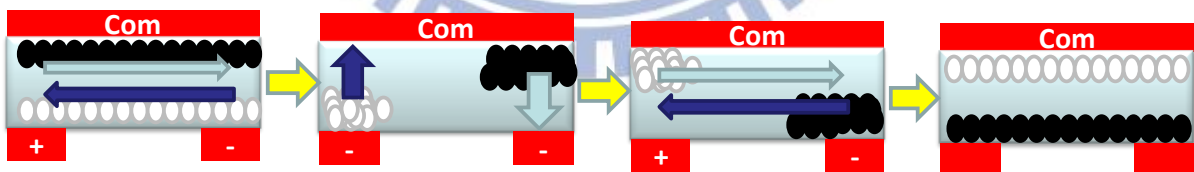


Fig. 5-12 The lateral reset could prevent collision by separating the particles.

The experimental results showed the waveform with the same 15 V 200 ms DC driving phase but different reset conditions. This driving waveform without reset only could push particles to the dark state about $L^* = 45$. The driving waveform with reset would push particles to the darker state about $L^* = 30$ as shown in Fig. 5-13. Moreover, the short term bistability lost in 30 seconds showed that the delta lightness (ΔL^*) were 0.3 and 0.8 with

and without reset respectively. In conventional driving waveforms, the short term bistability lost was $\Delta L^* \approx 1-2$ in 30 seconds. The bistability lost happened in 30 seconds mostly. Therefore, lateral reset made the transition quicker and more stable in the driving phase by creating a neutralized environment.

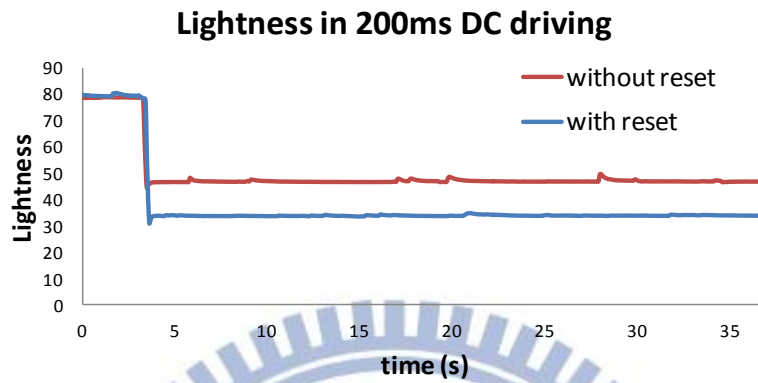


Fig. 5-13 The comparison of reset waveform.

Unlike vertical shaking, lateral shaking could recombine the ions without flicking effect by particles moved along lateral direction as Fig. 5-14. Consequently, using the lateral electric field in in-plane electrodes for lateral reset solved the flicking effect issue powerfully. Moreover, in this method, the image deviation of lateral reset was much smaller than that of vertical reset, so that people would only discover the image transition in reset part slightly as shown in Fig. 5-15. Nevertheless, the extreme state of the lateral driving was that particles swam to the electrodes. Therefore, the transition distance which was a 20 μm pitch of electrodes was shorter than a 30 μm cell gap. In the same electric field, transition time in reset process would be further reduced.

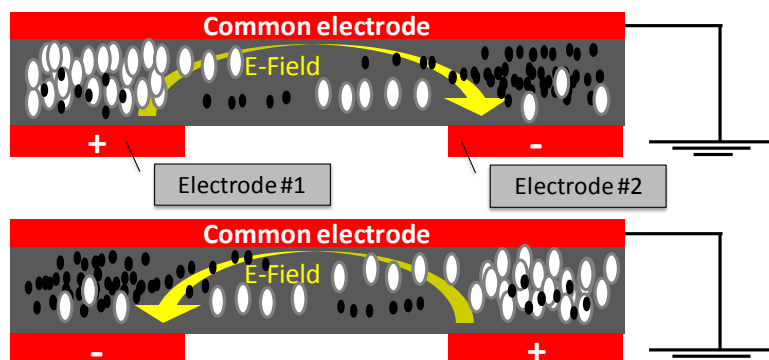


Fig. 5-14 The particles moving in the lateral reset.

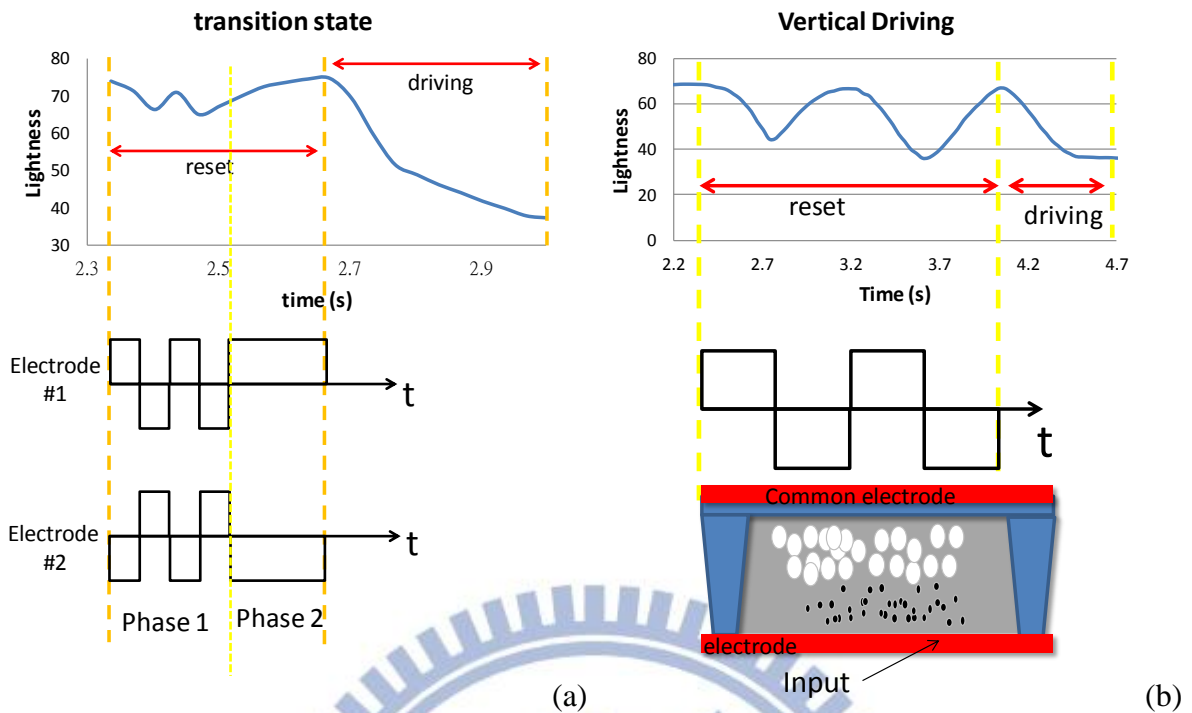


Fig. 5-15 Comparison of improved driving and vertical driving (a) Improved image transition including reset waveform (b) Vertical driving including reset.

5.2.2 Dual Side Driving Characteristic

Since there were two channels in a single pixel, switching images could only use one channel to build up the weaker electric field for image perturbation. By the non-uniform electric field, the force strength depended on the relative position of particles and electrodes. Therefore, after reset, one electrode side would pile the opposite charged particles and the other charged particles were close to the top of microcup as shown in Fig. 5-16, because the top layer had smaller electric field.

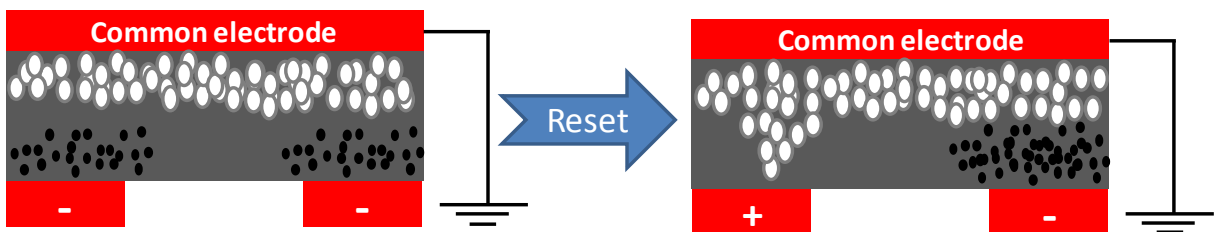


Fig. 5-16 The particles transition in reset waveform.

Single side driving used the weak electric field to affect the top site particles and switched the reflectivity slightly. This kind of driving could tune the difference of lightness in $\Delta L^* = 1$ as shown in Fig. 5-17. This film theoretically had gray levels larger than 64 from total $\Delta L^* > 64$ due to the limitation of the lightness between $L^* = 15$ to $L^* = 80$ by enough driving time which was larger than one second. Therefore, in achievable situation, the brightest lightness $L^* = 75$ and the darkest lightness $L^* = 25$, the 50 lightness variation was presented. The gray scales were triplet than current product. Next, the short term bistability lost in this method was $\Delta L^* < 1$ in 30 seconds by the partly lateral electric field as Fig. 5-18. The non-uniform electric field would eliminate the ions accumulation. Therefore, this driving method could reach the better short term bistability and more gray scales but the response was much slower than conventional ones. This driving method could be used as fine driving.

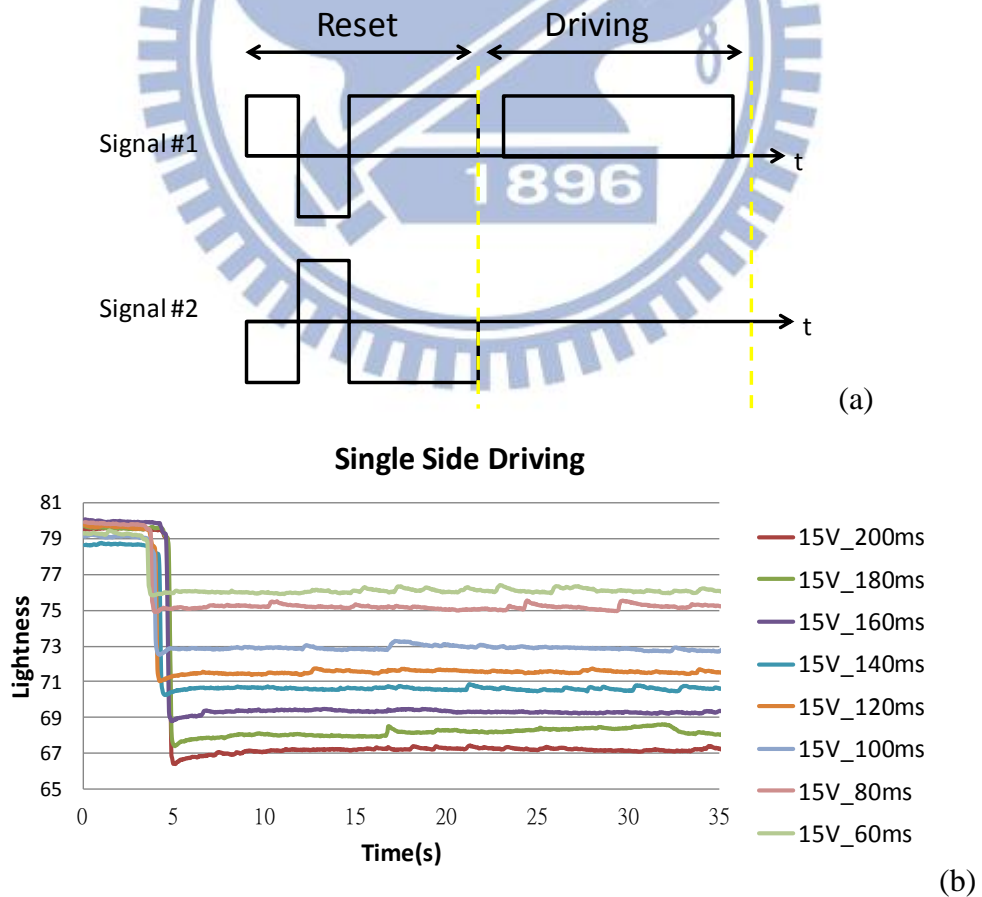


Fig. 5-17 The single side driving (a) waveform and (b) perturbs the lightness.

Single Side Driving

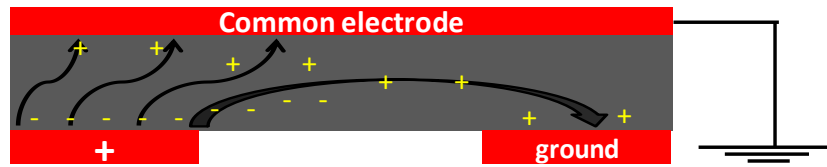
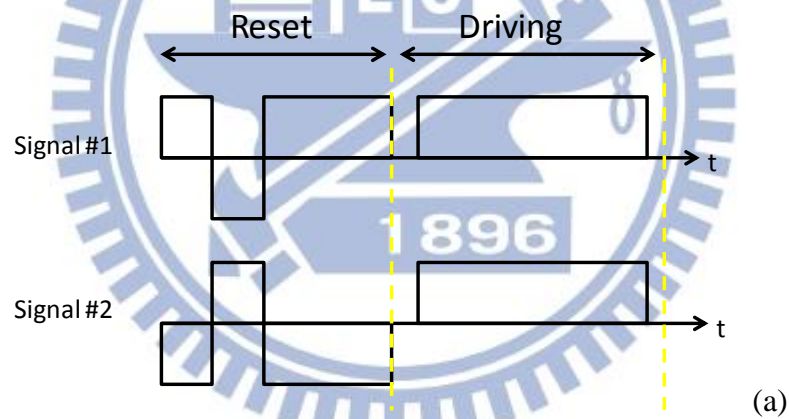


Fig. 5-18 The electric field distribution in single side driving.

There was another way to drive the particles faster by double side driving. The same signal would be applied to the two channels to distribute the stronger electric field than single side driving. In 15 V DC driving, 60 ms and 200 ms would decrease lightness from 80 to 62 and 80 to 35 as shown in Fig. 5-19. The response was quicker than single side driving. Combining single and double side driving, the lightness transition would be faster and more exquisite.



Double Side Driving

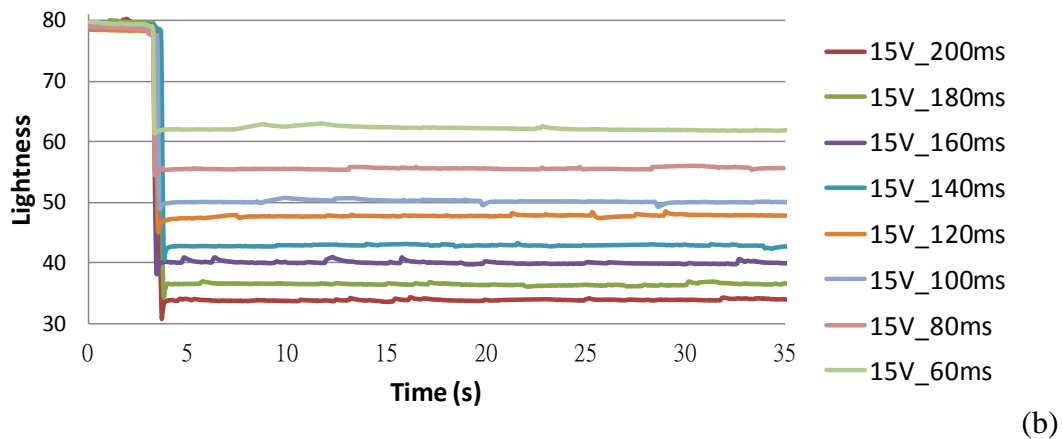


Fig. 5-19 The double side driving (a) waveform and (b) optical response.

However, double side driving method still had the slower response time than the conventional driving method because the electrode did not fill the full area on the substrate. Hence, there still had a little curved electric field to decrease the strength of vertical electric field. Therefore, dual side driving would enhance the image quality but decrease the response time. Consequently, using the larger voltage at the beginning of driving phase would compensate the slow response time issue from two channels driving.

As the result, the short term bistability lost was $\Delta L^* < 1$ by the non-uniform electric field as shown in Fig. 5-20. The ions could recombine at the central region and eliminate ions accumulation. It was still better than conventional one, and the response time was faster as shown in Fig. 5-21. Therefore, mixing 15 volt, 30 volt single and double driving would accomplish fast response, excellent short term bistability, $\Delta L^* < 1$, and more than 50 gray levels.

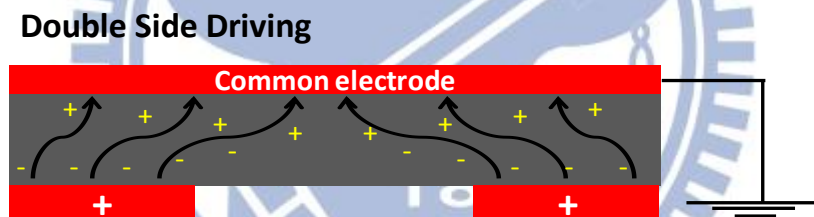


Fig. 5-20 The electric field distribution in double side driving.

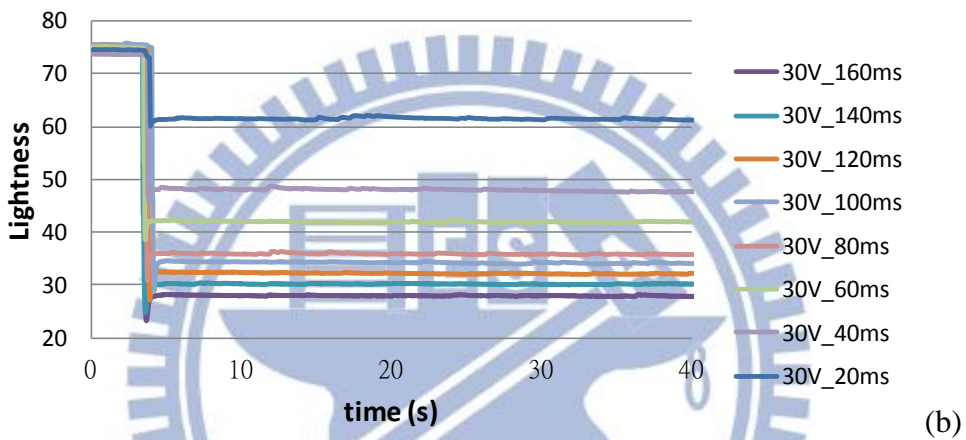
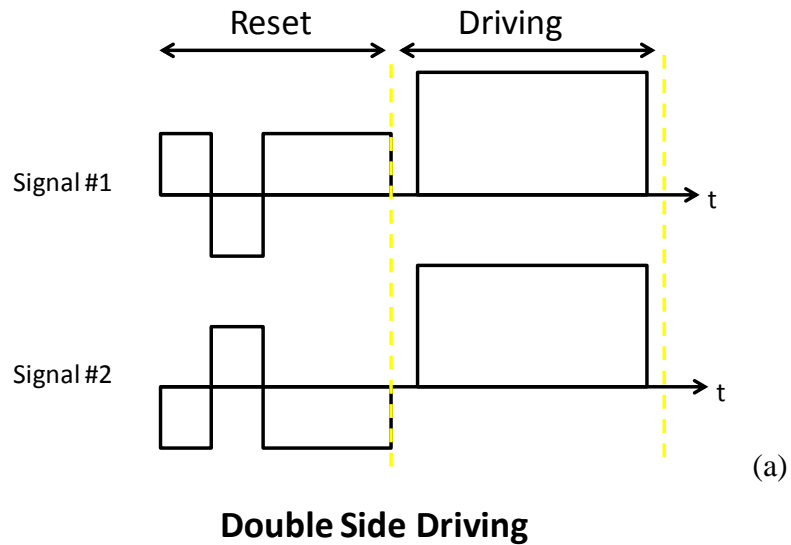


Fig. 5-21 The 30 volt double side driving (a) waveform and (b) optical response

From Section 5.1, the pulsing could be added after DC for the faster response, the less bistability lost, and the darkest or whitest state. The 15 V or 30 V pulsing after 30 volt DC would reach the darker state as shown in Fig. 5-22. The 30 volt pulsing could push the particles darker than 15 volt pulsing, but the short term bistability lost was larger. In 15 volt and 30 volt 20 ms pulsing, 30 volt was darker than 15 volt by $L^* \approx 2$. In 15 volt and 30 volt 40 ms pulsing, 30 volt was darker than 15 volt by $L^* < 1$. It meant the longer the driving time was, the fewer the lightness deviation in different driving voltage was. Moreover, the 30 volt pulsing added the short term bistability lost $\Delta L^* \approx 0.3$ in 30 seconds, the 15 volt pulsing only added the short term bistability lost $\Delta L^* \approx 0.1$ in 30 seconds.

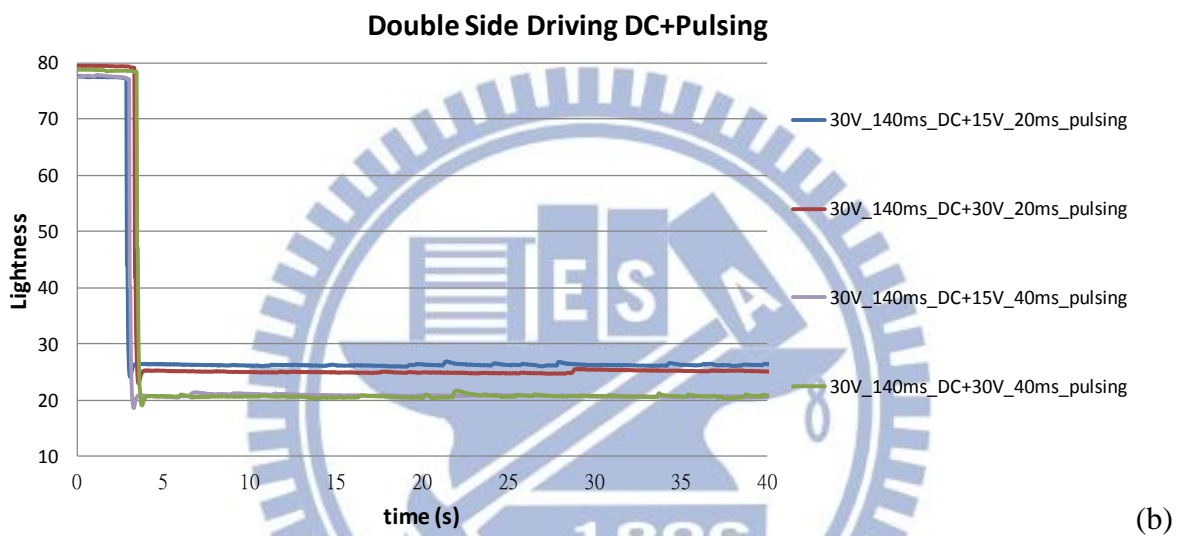
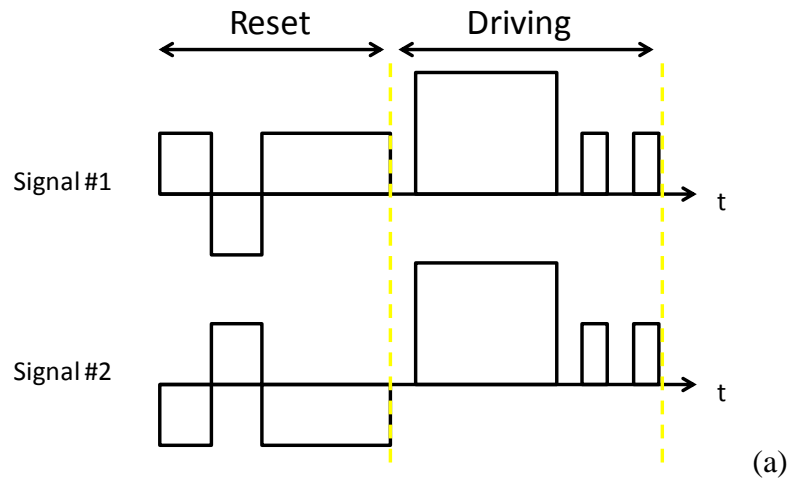


Fig. 5-22 The double side driving (a) waveform with 15 and 30 volt pulsing after 30 volt DC and (b) optical response.

Therefore, the lowest lightness could be achieved $L^* = 20$. The short term bistability lost could be minimized to $\Delta L^* \approx 0.1$ in 30 seconds. The response time without reset could be reduced to less than 220 ms even with reset by 500 ms from the whitest state to the darkest state. The in-plane electrode not only provided an excellent environment to accelerate the particles by the lateral electric field reset without flicker but also built up the multi-channel driving method to achieve more gray levels and excellent short term bistability. This driving method could be used as coarse driving.

The dual side driving provided the excellent short term bistability environment, and the fine-tunable gray levels. The single side driving provided the $\Delta L^* = 1$ precision to be the

fine adjustment. Therefore, more gray levels could be switched by this driving method. The double side driving made the particles transition faster for coarse adjusting. The stronger and more direct electric field was provided by double side driving. Moreover, the pulsing waveform after DC would further enhance the transition speed and the degree of extremely white or black state because the internal electric field was eliminated as Section 5.1.

By the driving phase mixing, a fast, accurate, and stable EPD driving waveform was proposed as shown in Fig. 5-23. At first, the reset driving phase recombined the opposite charged ions for eliminating the remnant DC inside the microcup by the last driving and separated the one type of particles to the electrodes for fast transition. Second, the coarse driving used larger voltage to increase the transition speed. Then, the pulsing was applied for minimizing the internal electric field to further increase the transition speed. Finally, the fine adjustment was applied at the end of the waveform. The single side driving provided a curved and weak electric field to drive the particles slightly and the lightness could be changed under a unit of lightness. Also, the single side driving provided the less internal electric field for better short term bistability. This proposed method improved the image quality as shown in Fig. 5-24.

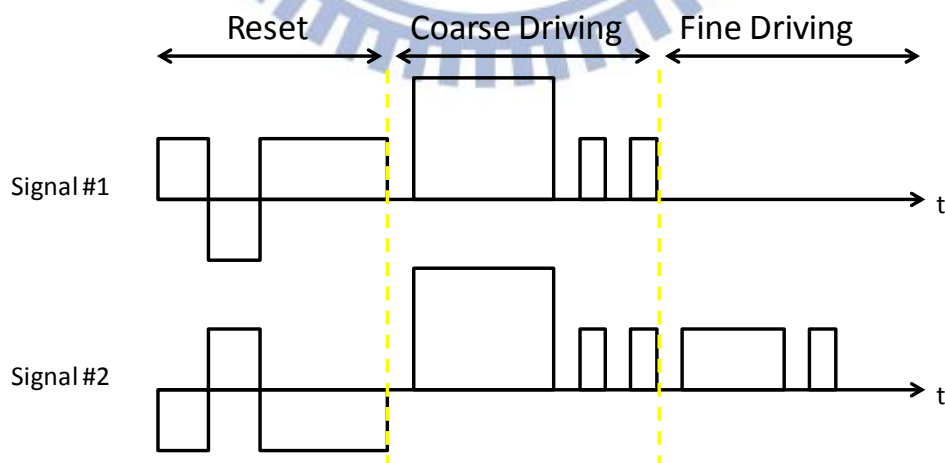


Fig. 5-23 The mixture waveform.

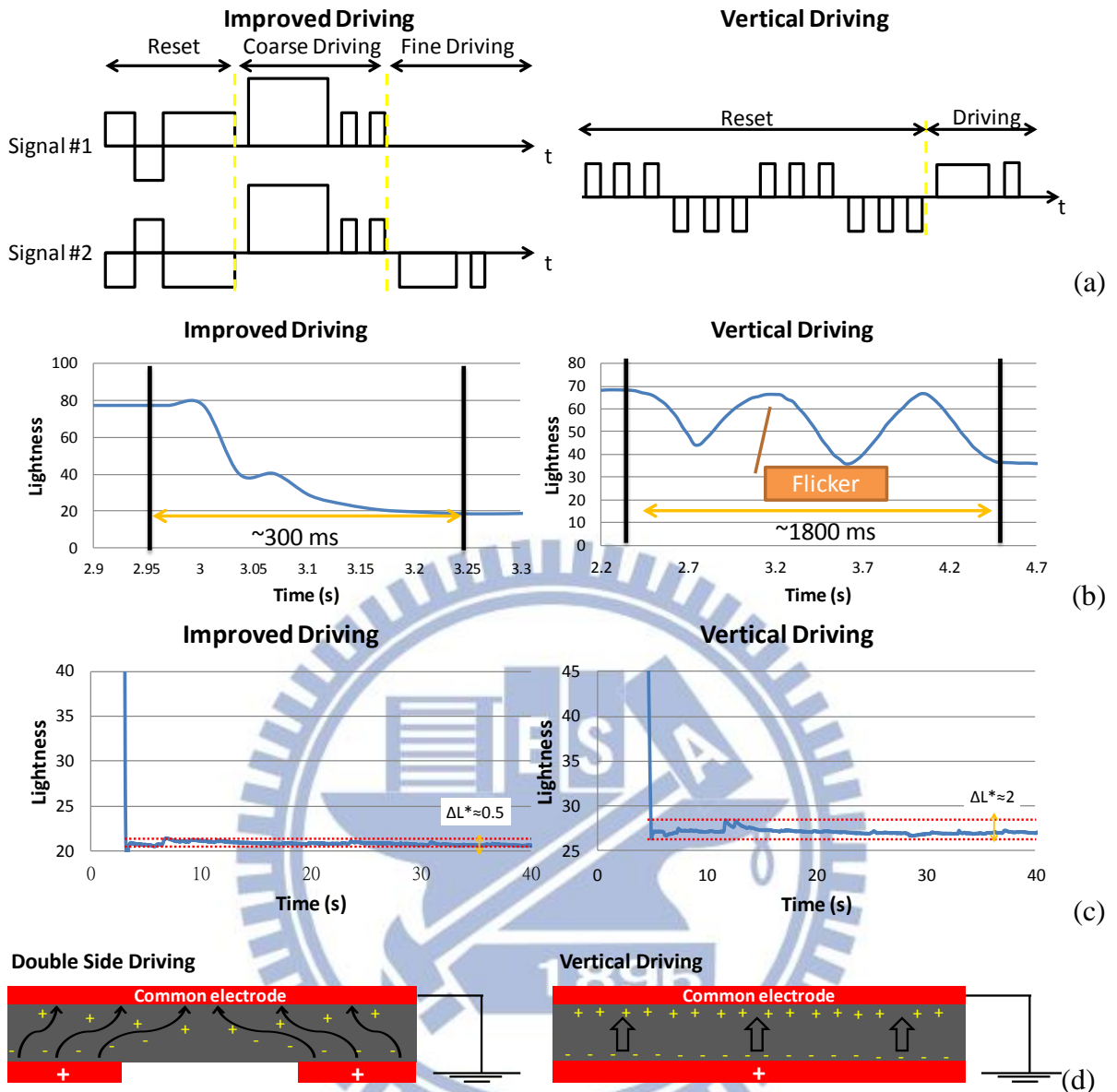


Fig. 5-24 Comparison of vertical driving and improved driving (a) driving waveform (b) flicker and response time (c) bistability and (d) its mechanism

Therefore, the image quality would be enhanced by eliminating the induced internal electric force from the curved electric field and lateral reset. The transition speed and the whitest and darkest state were improved by larger voltage and pulsing. The short term bistability was promoted by using lateral electric field. Moreover, the number of gray level was enhanced by one channel driving. Therefore, the lateral electric field from in-plane electrode was essential for the next generation EPD.

5.3 Summary

Experimental results of Section 5.2 showed lots of performance improvements as shown in Table 5-1. The flicker was eliminated from $\Delta L^* = 30$ to $\Delta L^* < 5$ by lateral shaking in lateral reset. The response time was shortened from 900 ms to 400 ms by lateral separation in lateral reset, higher driving voltage and pulsing. The short term bistability was enhanced from $\Delta L^* \approx 1-2$ to $\Delta L^* < 0.4$ in 30 seconds by curved electric field in dual side driving method. Moreover, the dual side driving method provided not only curved electric field but also optional driving electrode. Therefore, the number of gray levels was gained from 16 gray levels to least 32 gray levels.

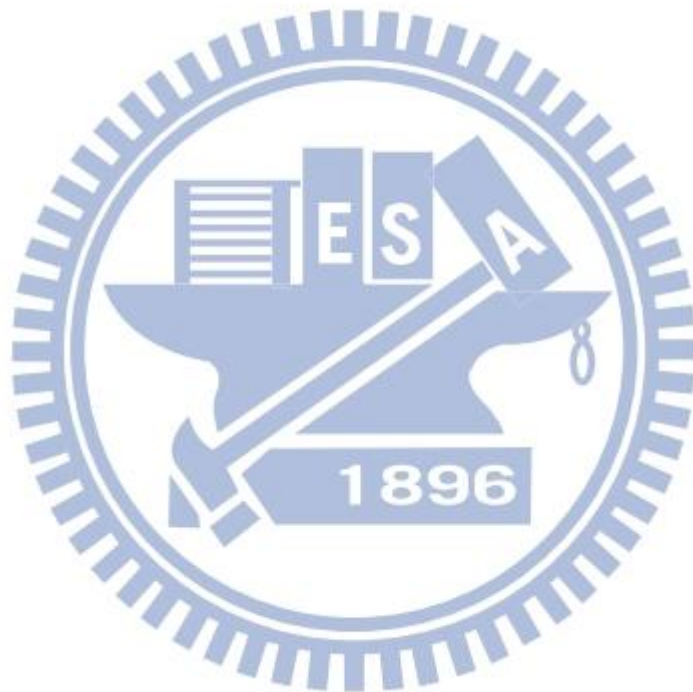
Table 5-1 The comparison of conventional and In-Plane EPDs.

	Current EPD	Objectives	Results
Response time	~700 ms	< 500 ms	~ 400 ms
Bi-stability	$\Delta L^* \sim 1-2$ in 30 seconds	$\Delta L^* < 1$ in 30 seconds	$\Delta L^* \sim 0.3$ in 30 seconds
Flicker	Uncomfortable $\Delta L^* \sim 30$	Invisible $\Delta L^* < 1$	Visible $\Delta L^* \sim 5$
Number of gray levels	16 gray levels	None	Least 32 gray levels

Consequently, the lateral driving method could carry lots of benefits. However, using in-plane electrode to provide lateral electric field needed two signals in one pixel. Therefore, two TFTs were needed in the same pixel. Therefore, the fabrication would be more difficult and expensive.

On the other hand, the pitch of electrodes: L would be the most important parameter. Because the smaller L would get higher electric field but lower working ratio. When L was small, the electric field would be larger and the electrode space would be larger too. It could

get faster response. However, the working ratio was low. Therefore, the flicker would be more serious and bistability would be decreased. Consequently, it was a tradeoff between response and flicker.



Chapter 6. Conclusion and Future Work

Electrophoretic display was one of the most important green technologies because of their bistability, flexibility, wide viewing angle and eco-friendly characteristics. However, electrophoretic displays suffer from their flicking effect, slow response time and non-perfect bistability; it is not the most popular display now. Nevertheless, several green displays were proposed to compete in the marketing such as OLED, ChLCD, and IMOD.

Therefore, the lateral driving method was proposed to overcome those issues by manipulating the electrophoretic particles in two directions. Dual side driving would produce higher bistability, faster response, and non-flicker transition. Moreover, this driving method would increase the number of gray levels to least 32 gray levels.

6.1 Conclusion

We proposed lateral driving method by using lateral and vertical electric field from in-plane electrode. The in-plane electrode was simulated for lateral electric field intensity and working ratio by tuning the electrode width (W) and pitch (L) as shown in Table 6-1. For stronger lateral electric field and larger working ratio, the W should be minimized. L was a tradeoff between lateral electric field strength and working ratio.

Table 6-1 The effects of W and L in the microcup EPD.

	Smaller W	Smaller L
E_x	stronger	stronger
Working Ratio	larger	smaller
Fabrication	hard	hard

From the mechanism understanding, when the voltage rose, the retardant force was raised too. Therefore, to provide a rest before driving was a method to eliminate the

retardant force and to make the transition time faster. The way of packing particle closer was using smaller voltage to prevent the repulsing force. And short term shaking would neutralize the opposite charged ions for better bistability.

Therefore, the driving method combined those abilities was proposed as Fig. 6-1. A higher voltage DC could be used at the very beginning. Then, pulsing came after the DC for the lower internal electric field by the short time rest. Shaking would appear for better bistability by neutralizing ions. Pulsing was given for the high contrast ratio by closely particle packing.

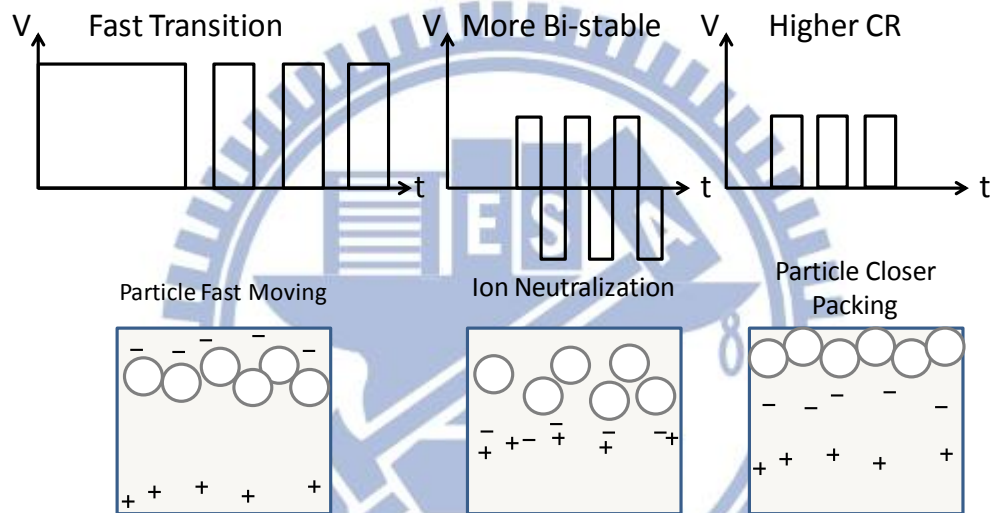


Fig. 6-1 The proposed waveform for quick response, high contrast ratio and stable lightness.

Consequently, the performance could be enhanced by minimizing the resistant force from the mechanism observation and measurement. The speed was improved by short time rest for ion self-neutralization to decrease the internal electric field. The bistability was promoted by shaking to combine opposite charged ions. The contrast ratio was enhanced by small voltage pulsing finally for the closest particle packing. Moreover, the mechanism was known by lateral observation method, so the material could be fine tune in the future.

Then, to apply the in-plane electrode as a pixel electrode, the lateral driving method was needed. The lateral driving method was proposed for the better image quality and no

flicking effect. The reset process was done in the lateral direction for the better short term bistability and faster driving phase. It would neutralize ions to eliminate the internal electric field and separate the particles for the non-collided transportation as shown in Fig. 6-2. The white particles went down and black particles went up. They collided with each other without lateral reset. Consequently, the lateral reset process was essential for the in-plane electrode to be a pixel electrode of next generation EPD.

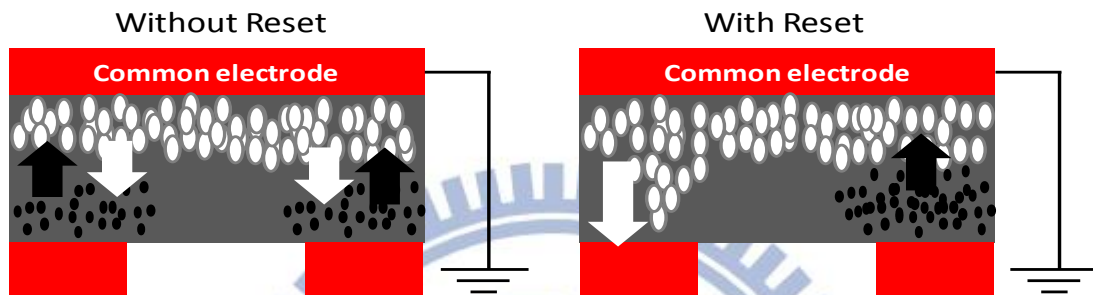


Fig. 6-2 The particles transition direction.

The gray levels could be more stable and added by dual side driving. Image transition could do the coarse driving to the nearly gray level by double side driving in 30 V DC and 15V pulsing as shown in Fig. 6-3, and then do the fine driving to the exact gray level by single side driving as shown in Fig. 6-4. Moreover, single side driving could reach better bistability. Therefore, using this driving method would get good bistability, fast response, and more gray levels.

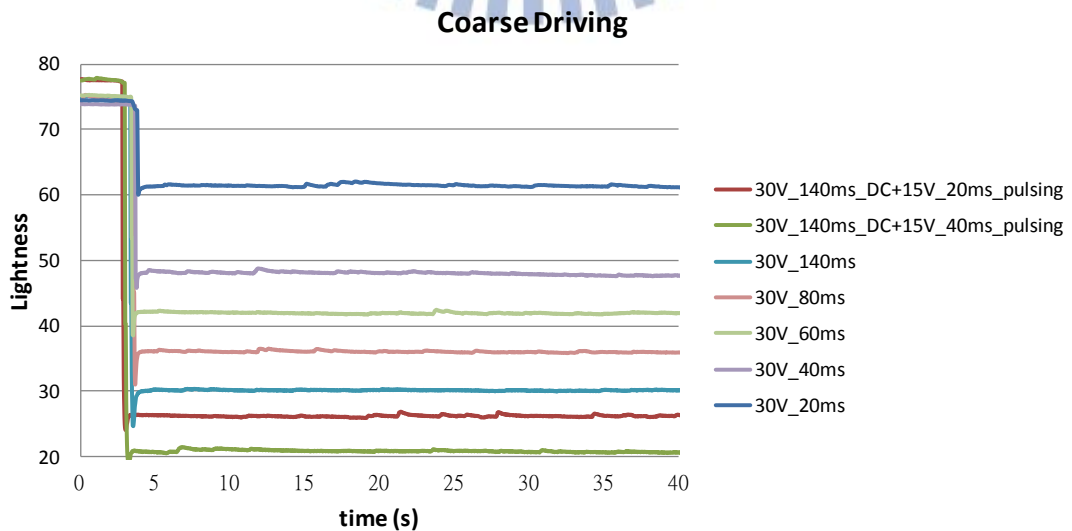


Fig. 6-3 The coarse adjustment.

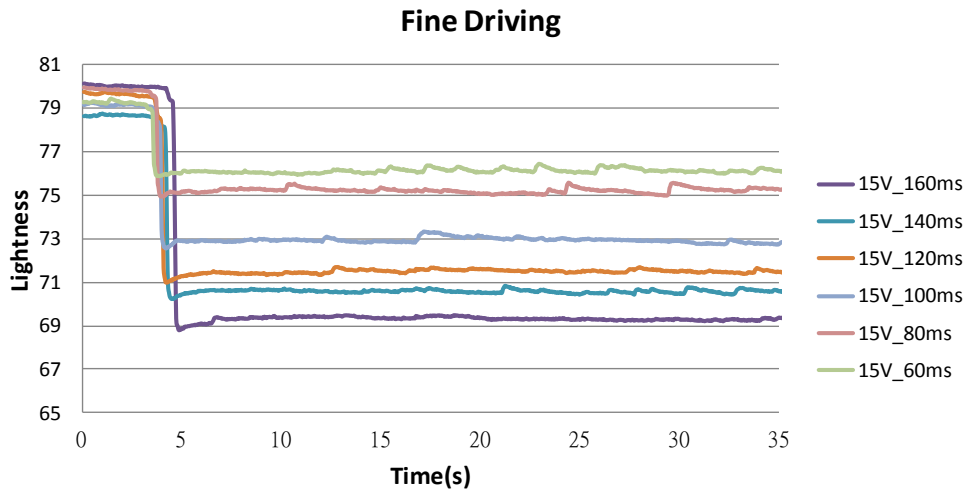


Fig. 6-4 The fine adjustment.

Therefore, the image quality would be enhanced by eliminating the induced internal electric force from the curved electric field and lateral reset as shown in Table 6-2. The transition speed and the whitest and darkest state were improved by larger voltage and pulsing. The bistability was promoted by using lateral electric field. Moreover, the number of gray level was enhanced by one channel driving. So, the lateral electric field from in-plane electrode was essential for the next generation EPD.

Table 6-2 The improvement of the microcup EPD.

	Current EPD	Dual Side Driving Method	Accomplishment
Response time	~700 ms	~ 400 ms	●
Bi-stability	$\Delta L^* \sim 1-2$ in 30 seconds	$\Delta L^* \sim 0.3$ in 30 seconds	★
Flicker	Uncomfortable $\Delta L^* \sim 30$	Visible $\Delta L^* \sim 5$	▲
Number of gray levels	16 gray levels	Least 32 gray levels	★

★ Excellent

● Good

▲ Acceptable

6.2 Remnant Issue and Future Work

Lateral electric field was simulated and observed by microscopic system. Moreover, the lateral driving method was proposed for the higher image quality. However, the flicker was still visible because the vertical electric field in lateral reset. Therefore, electrode could be designed in another shape to build up different distribution of electric field and eliminating flicker by reducing the area where contributing the vertical electric field.

Moreover, the complex driving waveform and electrode design were not attempted yet. For example, the gray level to gray level direct driving method as shown in Fig. 6-5 was not researched deeply. By doing so, the transition speed would be increased as well.

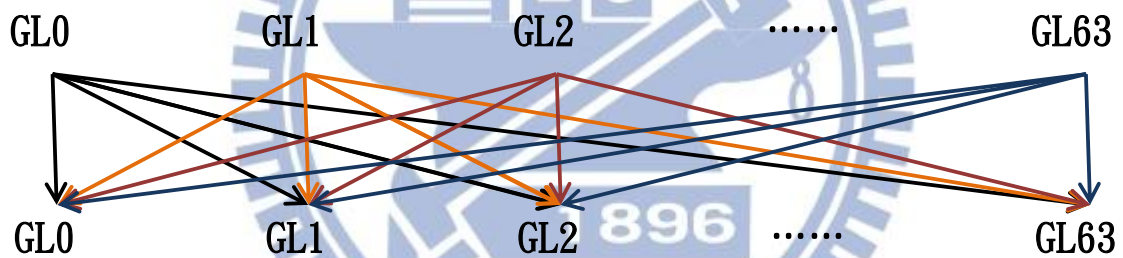


Fig. 6-5 The gray level transition web.

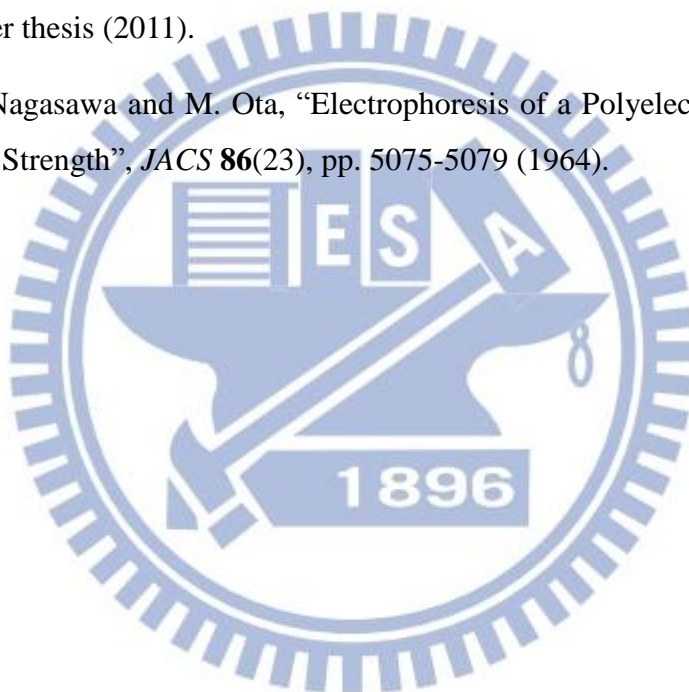
Furthermore, tuning material parameters is also a powerful method. The transition speed and bistability are primary confined by the materials, and they are tradeoff. Therefore, reaching the balance of speed and bistability is a big issue. Then, assisting the performance by the electrode structures and driving waveforms would make electrophoretic display to be a popular display in the marketing.

References

- [1] A. L. Dalisa, "Electrophoretic display technology", *IEEE Electron Devices* **24**(7), pp. 827-834 (1977).
- [2] R.M.A Dawson, et al, "The impact of the transient response of organic light emitting diodes on the design of active matrix OLED displays", *IEDM Technical Digest*, pp. 875-878 (1998).
- [3] Russel A. Martin, "Driving mirasol® Displays: Addressing Methods and Control Electronics", *SID Symp. Digest Tech Papers* **42**, pp. 330-333 (2011).
- [4] Ivan Dozov, et al, "Recent improvements of bistable nematic displays switched by anchoring breaking (BiNem)", *SID Symp. Digest Tech Papers* **16**, pp. 224-227 (2001).
- [5] Donald L White, et al, "New absorptive mode reflective liquid-crystal display device", *JAP* **45**, Issue 11, pp. 4718 -4723 (1974).
- [6] Jacob H. Masliyah, "Electrokinetic and colloid transport phenomena", Hoboken, NJ : J. Wiley (2006).
- [7] Joseph M. Jacobson, et al, "Electrophoretic displays using nanoparticles", *US Patent*, No. 6538801 B2 (2003).
- [8] Joseph M. Jacobson, "Electronically addressable microencapsulated ink and display thereof", *US Patent*, No. 6120588 (2000).
- [9] Paul Drzaic and Russell J. Wilcox, "Full color reflective display with multichromatic sub-pixels", *US Patent*, No. 7075502 B1 (2006).
- [10] Reiji Hattori, et al, "Distinguished Paper: Ultra Thin and Flexible Paper-Like Display using QR-LPD® Technology", *SID Symp. Digest Tech Papers* **10**, pp. 136-139 (2004).
- [11] Ryo Sakurai, et al, "Color and Flexible Electronic Paper Display using QR-LPD® Technology", *SID Symp. Digest Tech Papers* **37**, pp. 1922-1925 (2006).
- [12] Jerry Chung, et al, "Microcup® Electrophoretic Displays, Grayscale and Color Rendition", *IDW* **10**, pp. 243-246 (2003).

- [13] R. C. Liang, et al, "Microcup® displays: Electronic paper by roll-to-roll manufacturing processes", *JSID* **11**(4), pp. 621-628 (2003).
- [14] Barrett Comiskey, et al, "An electrophoretic ink for all-printed reflective electronic displays", *Nature* **394**, pp. 253-255 (1998).
- [15] T. Bert and H. De Smet, "Dielectrophoresis in electronic paper", *Displays* **24**(4-5), pp. 223-230 (2003).
- [16] V. Novotny and M. A. Hopper, "An electrophoretic display, its properties, model, and addressing", *IEEE Electron Devices* **26**(8), pp. 1148-1152 (1979).
- [17] T. Bert, et al, "Complete electrical and optical simulation of electronic paper", *Displays* **27**(2), pp.50-55 (2006).
- [18] Szu-I Wu, et al, "Electrokinetics of Charged-Particles in Microcup Electrophoretic Displays", *SID Symp. Digest Tech Papers* **42**, pp. 1559-1562 (2011).
- [19] T. Bert, et al, "Steady state current in EPIDs", *Displays* **27**(1), pp.35-38 (2006).
- [20] E. Kishi, et al, "Development of In-Plane EPD", *SID Symp. Digest Tech Papers* **31**, pp. 24-27 (2000).
- [21] H. Yoshinaga and S. Itabashi, "Panel for display device, and display device", *US Patent*, No. 20050285843 A1 (2005).
- [22] K. Nagayama, "Electrophoretic display apparatus and driving method thereof", *US Patent*, No. 20070120812 A1 (2007).
- [23] Andrew L. Dalisa and Robert J. Seymour, "Electrophoretic display devices", *US Patent*, No. 4218302 (1980).
- [24] Mark T. Johnson, et al, "In-plane switching electrophoretic display devices", *US Patent*, No. 20050275933 (2005).
- [25] Jerry Chung and David Chen, "Electrophoretic display with gating electrodes", *US Patent*, No. 6781745 B2 (2004).
- [26] Rong-Chang Liang and Jerry Chung, "Electrophoretic display with dual mode switching", *US Patent*, No. 7038670 B2 (2006).

- [27] C. J. Chung, “Dispersion of titania powder in an electronic ink for electrophoretic display”, NTHU, Master thesis (2007).
- [28] T. Bert and H. De Smet, “How to introduce a threshold in EPIDs “, *IDRC*, pp. 337-339 (2005).
- [29] P. C. Hsu, “In-Plane Lateral Driving Phenomena in Electrophoretic Displays”, *SID Symp. Digest Tech Papers* **63**, pp. 1357-1360 (2012).
- [30] P. C. Hsu, “Analysis Optical Response of E-paper by Lateral Operation”, *TDC* pp. 61-64 (2012).
- [31] S. I. Wu, “Electrokinetics of Charged-Particles in Microcup Electrophoretic Displays”, NCTU, Master thesis (2011).
- [32] I. Noda, M. Nagasawa and M. Ota, “Electrophoresis of a Polyelectrolyte in Solutions of High Ionic Strength”, *JACS* **86**(23), pp. 5075-5079 (1964).



Publication List

International Conference Papers

1. **Po-Chun Hsu**, Fang-Cheng Lin, Yi-Pai Huang, Han-Ping D. Shieh, and Shie-Chang Jeng, “In-Plane Lateral Driving Phenomena in Electrophoretic Displays”, Society for Information Display 2012 (SID’12), pp. 1357~1360.

Domestic Conference Papers

1. **Po-Chun Hsu**, Fang-Cheng Lin, Yi-Pai Huang, Han-Ping D. Shieh, and Shie-Chang Jeng, “Analysis Optical Response by Lateral Operation”, Taiwan Display Conference 2012 (TDC2012) pp. 61~64.

